npj | Parkinson's Disease

www.nature.com/npjparkd

ARTICLE OPEN

Check for updates

High content screening and proteomic analysis identify a kinase inhibitor that rescues pathological phenotypes in a patient-derived model of Parkinson's disease

Nasia Antoniou[1,2], Kanella Prodromidou[1], Georgia Kouroupi[1], Ioanna Boumpoureka[1], Martina Samiotaki[3], George Panayotou[3], Maria Xilouri[4], Ismini Kloukina[4], Leonidas Stefanis[4,5], Regis Grailhe[6], Era Taoufik[1,7] and Rebecca Matsas[1,7]✉

Combining high throughput screening approaches with induced pluripotent stem cell (iPSC)-based disease modeling represents a promising unbiased strategy to identify therapies for neurodegenerative disorders. Here we applied high content imaging on iPSC-derived neurons from patients with familial Parkinson's disease bearing the G209A (p.A53T) α-synuclein (αSyn) mutation and launched a screening campaign on a small kinase inhibitor library. We thus identified the multi-kinase inhibitor BX795 that at a single dose effectively restores disease-associated neurodegenerative phenotypes. Proteomics profiling mapped the molecular pathways underlying the protective effects of BX795, comprising a cohort of 118 protein-mediators of the core biological processes of RNA metabolism, protein synthesis, modification and clearance, and stress response, all linked to the mTORC1 signaling hub. In agreement, expression of human p.A53T-αSyn in neuronal cells affected key components of the mTORC1 pathway resulting in aberrant protein synthesis that was restored in the presence of BX795 with concurrent facilitation of autophagy. Taken together, we have identified a promising small molecule with neuroprotective actions as candidate therapeutic for PD and other protein conformational disorders.

npj Parkinson's Disease (2022)8:15 ; https://doi.org/10.1038/s41531-022-00278-y

INTRODUCTION

Parkinson's disease (PD) is a complex neurodegenerative disorder affecting 2% of the world population over 65 years of age[1]. PD is characterized by motor dysfunction related to the progressive loss of midbrain dopamine neurons[2] while a wide range of non-motor symptoms are also present such as psychiatric manifestations and cognitive impairment[3]. The neuropathological hallmark of PD is the presence of intracytoplasmic inclusions in neuronal cell bodies and neurites, respectively termed Lewy bodies and Lewy neurites[4,5]. These are protein aggregates composed mainly of α-synuclein (αSyn), the major protein linked to sporadic PD[6]. αSyn belongs to a class of intrinsically disordered amyloid proteins that form specific forms of oligomeric and fibrillar aggregates and exert neurotoxicity through various molecular pathways[7]. Several point mutations (A30P, E46K, A53T, G51D) and multiplications of the *SNCA* locus encoding for αSyn cause autosomal dominant forms of PD[8–10]. Among the different variants, the p.A53TαSyn mutation is generally considered to accelerate aggregation[11] resulting in widespread accumulation of insoluble α-syn deposits that have been identified in the post-mortem p.A53T human brain[12,13]. Despite extensive efforts in understanding PD pathogenesis, no disease modifying drugs exist. Currently only symptomatic or palliative treatments are available with none capable to prevent or slow-down disease progression. Dopamine-replacement drugs, such as levodopa, which was identified 53 years ago[14], are used to ameliorate motor symptoms and remain the primary and most effective treatment despite the undesired side-effects and deterioration of efficacy with disease progression. Therefore, the development of disease-modifying drugs is an urgent unmet need. Most present-day efforts in identifying PD therapeutics target the aggregation of misfolded αSyn as the major pathogenic factor that causes cellular toxicity[6,15–17]. Alternative strategies to tackle early steps in neurodegeneration, particularly in an unbiased approach, have lagged behind. Recent advances in patient-derived induced pluripotent stem cell (iPSC)-based models for neurodegenerative diseases permit the detection of early, potentially triggering, pathologic phenotypes and provide amenable systems for drug discovery. In combination with high throughput high content screening technologies, these approaches open new perspectives for identification of disease-modifying compounds[18–21].

We have previously established a model of iPSC-derived neurons from patients with familial PD harboring the p.A53T αSyn mutation (G209A in the *SNCA* gene) that displays disease-relevant phenotypes at basal conditions[22]. In this study, we successfully adapted this cellular system to perform a small molecule screen on human p.A53T-neurons and discovered that the multi-kinase inhibitor BX795 significantly reverts disease-associated phenotypes. A single treatment of patient neurons with BX795 has sustainable effects in supporting neuritic growth, restoring axonal pathology and limiting αSyn protein aggregate formation. Protection from p.A53T-associated pathology was also confirmed in human iPSC-derived neurons in which the mutation was introduced by genome editing, against isogenic wild-type

[1]Laboratory of Cellular and Molecular Neurobiology-Stem Cells, Hellenic Pasteur Institute, 127 Vassilissis Sofias Avenue, 11521 Athens, Greece. [2]Division of Animal and Human Physiology, Department of Biology, National & Kapodistrian University of Athens, Panepistimioupolis, Ilisia, Greece. [3]Institute of Bioinnovation, Biomedical Sciences Research Center "Alexander Fleming", Vari 16672, Greece. [4]Center of Clinical Research, Experimental Surgery and Translational Research, Biomedical Research Foundation of the Academy of Athens (BRFAA), 4 Soranou Efesiou Street, 11527 Athens, Greece. [5]1st Department of Neurology, Eginition Hospital, Medical School, National and Kapodistrian University of Athens, Athens, Greece. [6]Technology Development Platform, Screening Sciences & Novel Assay Technology, Institut Pasteur Korea, Bundang-gu, Seongnam-si, Gyeonggi-do 463-400, Republic of Korea. [7]These authors contributed equally: Era Taoufik, Rebecca Matsas. ✉email: rmatsa@pasteur.gr

Published in partnership with the Parkinson's Foundation

npj nature partner journals

Parkinson's Foundation

controls. Strikingly, proteomics profiling by quantitative mass spectrometry revealed that BX795 treatment results in significant downregulation of a cohort of 118 proteins that are abnormally upregulated in p.A53T-neurons. Enrichment analysis demonstrated that these proteins are associated with mRNA metabolism, mRNA transport and translation, protein metabolism and degradation processes. Using neuronal cells expressing the human p.A53T-αSyn, we demonstrate that BX795 affects the mTORC1 pathway to restrict excessive protein synthesis and facilitate autophagy. Taken together, our data highlight the BX795 kinase inhibitor as a compelling compound and candidate therapeutic that ameliorates p.A53T-related pathology.

RESULTS

Assay development for high-content screening of p.A53T-iPSC derived neurons

iPSCs used in this study were previously generated from a PD patient bearing the p.A53T αSyn mutation and thoroughly characterized[22]. For directed differentiation a dual SMAD inhibition protocol was used in the presence of Noggin and TGFβ inhibitor[22–24], which favors the generation and expansion of Pax6+/Nestin+ neural progenitor cells (NPCs; Fig. 1a). NPCs were further differentiated into βIII-tubulin (TUJ1)+ neurons (Fig. 1a) with 15-20% also expressing the dopaminergic marker TH at 21 DIV (Fig. 1a). The expression of dopaminergic lineage markers, such as Nurr1, TH, and aromatic amino acid decarboxylase (AADC) was confirmed by qRT-PCR (Supplementary Fig. 1). As readout for compound screening, we assessed TH immunofluorescence in iPSC-derived neurons adapted in miniature 384-well plates, seeking to identify putative neuroprotective compounds enhancing dopaminergic neuron output. To this end, the fluorescent signal for TH within a well was normalized to the fluorescent signal for the pan-neuronal marker βIII-tubulin (TUJ1) (Fig. 1b), allowing to monitor changes in the TH population in a simple and effective way.

High content screening of a kinase inhibitor library identifies BX795 as a compound that increases TH immunofluorescence in p.A53T-neurons

Protein kinases represent central molecular hubs that regulate numerous cell processes, thus constituting potentially attractive clinical targets. Indeed, the success of kinase inhibitors in treating cancer has spurred the evaluation of such compounds in phase II/III clinical trials as candidates for treatment of various neurodegenerative diseases[25,26]. Since several kinases have been implicated in PD pathology[27], we screened a collection of 273 small molecule kinase inhibitors (Supplementary Table 1) to identify compounds with prospective neuroprotective properties. p.A53T cells were exposed once (7 DIV) to the library of kinase inhibitors at 1 μM concentration and quantitative image analysis was performed at 21 DIV (Fig. 1a). Hits were defined as compounds that robustly conferred an increase in TH immunofluorescence compared to DMSO-treated p.A53T neurons within a well, normalized to the immunofluorescence of the pan-neuronal marker βIII-tubuin (TUJ1) (Fig. 1b, Supplementary Fig. 2). Toxic compounds were excluded by assessing cellular viability (total nuclei count) of compound-treated as compared to DMSO-treated cells (Supplementary Fig. 3). Four hits were identified in the primary screen (Fig. 1b), which were re-tested for validation in a dose-response assay (Fig. 1d). Of these, only BX795, an aminopyrimidine compound that acts as a multi-kinase inhibitor with pro-survival and/or anti-inflammatory action[28], showed a consistent dose-response effect and significantly increased TH immunofluorescence at 1 μM (Fig. 1c, d). BX-795 was initially developed as an ATP-competitive inhibitor of 3-phosphoinositide-dependent kinase 1 (PDK1), but was later shown to inhibit the IKK-related kinase, TANK-binding kinase 1 (TBK1) and IKKε, as well as to have numerous additional targets[29–31]. Based on the sustained effect of a single dose of BX795 on p.A53T dopaminergic neurons (Fig. 1d), we focused further on this compound to explore its function.

BX795 rescues neuropathological features of p.A53T neurons

The effects of BX795 on p.A53T-neurons were tested in cells that received a single treatment of the kinase inhibitor (1 μM) at 7 DIV and were analyzed at 21 DIV, in accordance with the protocol applied during the screening procedure. Prior to this, an initial set of experiments was performed using drug concentrations from 0.1-2 μM and repeated drug additions every 3 days, with the selected scheme ensuring optimal efficacy and minimal toxicity. Initially, we asked if the enhancement in TH immunofluorescence could be attributed to an increase in cell survival/proliferation or dopaminergic differentiation in p.A53T-cultures. We could not detect BX795-driven changes in either proliferation, as assessed by the percentage of Ki67+ cells (Supplementary Fig. 1; % Ki67+ cells, DMSO: 43.3 ± 4.4; BX795: 50.3 ± 1.5, $n = 3$), or in differentiation as estimated by the percentage of TH+ cells in the culture (% TH+/TUJ1+ neurons, DMSO: 13.9 ± 3.1; BX795: 18.1.0 ± 3.9, $n = 3$). Moreover, we did not detect any change in total cell viability, as assessed b nuclei count (Supplementary Fig. 1). These observations indicate that the effect of BX795 on dopaminergic neurons is not related to an increase in either survival/proliferation or differentiation.

Next, we investigated if treatment with BX795 could rescue neuropathological features previously identified in p.A53T-neurons, such as compromised neuritic growth, dystrophic or fragmented neurites and the presence of intracellular protein aggregates[22,32]. Overall, disease-associated phenotypes were assessed in iPSC-derived neurons from two p.A53T patients [22] and an iPSC gene-edited line in which the p.A53T mutation was inserted in one allele, against healthy or isogenic controls. Evaluation of total neurite length in TH+ dopaminergic neurons from the first p.A53T patient revealed a significant increase in response to BX795 compatible with the observed increase in TH immunofluorescence (length in μm, ctl: 221.7 ± 16.8, p.A53T:127.2 ± 13.5, p.A53T + BX795: 196.8 ± 21.1, $n = 5$, Fig. 2a). Moreover, examination of the distinct pathological morphology of TUJ1+ p.A53T neurons revealed an almost 50% reduction in axonal degeneration (axon degeneration index: ctl: 2.945 ± 1.325, p.A53T:13.03 ± 1.491, p.A53T + BX795: 7.276 ± 1.017 $n = 3$; Fig. 2b). Finally, exposure to BX795 resulted in a notable 60% decrease in protein aggregate formation in p.A53T cells (number of aggregates per cell, ctl: 2.384 ± 0.89, $n = 30$, p.A53T: 8.431 ± 0.77, $n = 51$, p.A53T+ BX795: 3.242 ± 0.40, $n = 62$; Fig. 2c). This was accompanied by a consistent decline in the levels of (Ser129)-phosphorylated αSyn (Fig. 2d), a modification that renders αSyn prone to self-assembly and is commonly associated with synucleinopathy[33,34]. The neuroprotective effects of BX795 were confirmed in p.A53T-neurons from a second patient[22,32] (Supplementary Fig. 4).

We also assessed the neuroprotective effects of BX795 in a highly enriched culture of mature human midbrain dopaminergic neurons (Fujifilm Cellular Dynamics Inc). These comprised an isogenic pair of wild-type (iCell DOPA) and gene-edited (iCell A53T DOPA) iPSC-derived neurons in which a heterozygous p.A53T mutation was inserted into one allele of the *SNCA* gene. After 14 days, more than 90% of cells were TUJ1+ and more than 80% were TH+ dopaminergic neurons (Fig. 3a). At this time and similarly to patient-derived cells, abundant protein aggregates were detected in the p.A53T iCell neurons compared to their isogenic control, and treatment with BX795 resulted in a significant reduction (number of aggregates per cell, ctl:2.7 ± 0.49, $n = 57$, p.A53T: 9.9 ± 1.1, $n = 76$, p.A53T+ BX795:4.9 ± 0.7, $n = 76$; Fig. 3b, c).

Taken together our results indicate that BX795 exerts prominent and sustainable neuroprotection in p.A53T neurons by improving

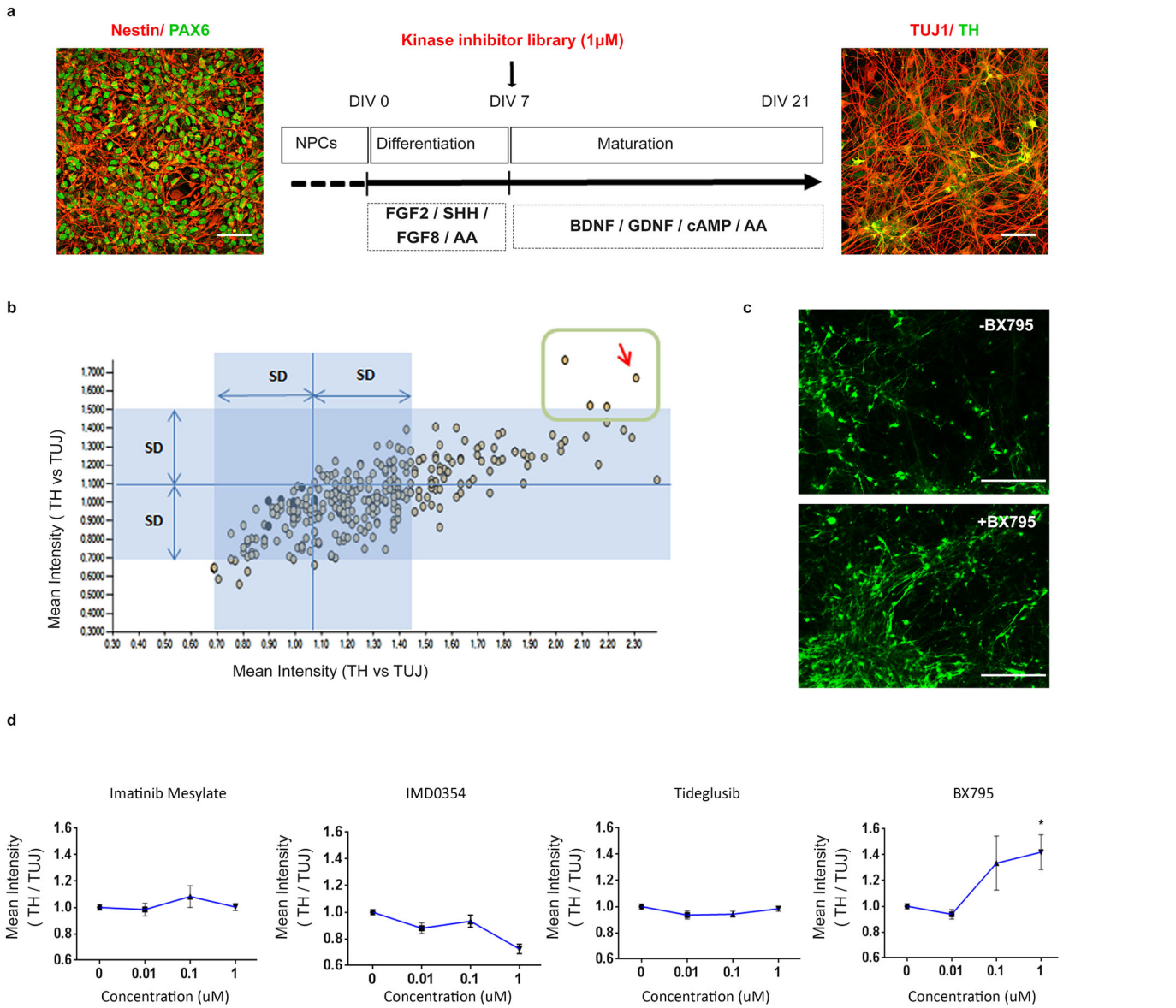

Fig. 1 Identification of BX795 by high content screening of a kinase inhibitor library. a Directed differentiation of Pax6+ (green)/Nestin+ (red) neural precursor cells (NPCs; DIV 0, left) into TUJ1+ (red)/ TH+ (green) neurons (DIV 21, right). The differentiation protocol and timeline of analysis are shown in the drawing in the middle. FG2 and FGF8, fibroblast growth factors 2 and 8; SHH Sonic Hedgehog, AA ascorbic acid, Scale bar represents BDNF brain-derived neurotrophic factor, GDNF glial cell-derived neurotrophic factor (GDNF), cAMP cyclic AMP. Scale bars, 50 μm. **b** Scatter plot showing the ratio of TH versus TUJ1 fluorescence intensity in duplicate upon treatment with 273 small molecule kinase inhibitors. The dots inside the green square correspond to the 4 hit compounds showing significant increase of TH versus TUJ1 fluorescence ratio as compared to the DMSO controls (blue dots). The red arrow indicates BX795. **c** Representative images of patient-derived p.A53T-neurons immunolabelled for TH in 384-well plates. Upper micrograph shows control DMSO-treated cells while lower micrograph represents BX795-treated cells. Scale bar represents 150 μm. **d** Tests of the four hit compounds in a dose-response format. Data are presented as mean ± SEM. (one-way ANOVA, $*P < 0.05$, $n = 3$ independent experiments).

neuritic growth, limiting the levels of pathological αSyn and restricting aggregate formation whilst maintaining axonal integrity. The beneficial effects of BX795 were noted whether it was added early during neuronal differentiation (in p.A53T patient-derived neurons) or at later stages of neuronal maturation (in A53T iCell dopaminergic neurons) when disease-associated phenotypes were already established.

Proteomics analysis identifies cellular pathways targeted by BX795 in p.A53T neurons

Identification of the BX795 affected cellular pathways which vary according to the system investigated[30,31,35], is a challenging task. Therefore, we used an unbiased approach based on comparative proteomics. Similarly to the screening procedure, BX795 was added once at DIV 7 and proteomics analysis was performed at DIV 21 when rescue of neuropathological phenotypes was noted (Fig. 2). A total of 1652 proteins were identified and quantified using the MaxQuant software[36,37], followed by filtering of low quality protein hits with the Perseus software. Initial comparison between p.A53T versus control neurons in the absence of BX795, revealed differential expression of 640 proteins (Supplementary Fig. 5) from which only 67 were down-regulated whilst the rest 573 were up-regulated (Supplementary Fig. 5, Supplementary Table 2). This large increase in protein expression was linked by GO enrichment analysis mainly to the biological processes of transcription, translation, protein synthesis and modification

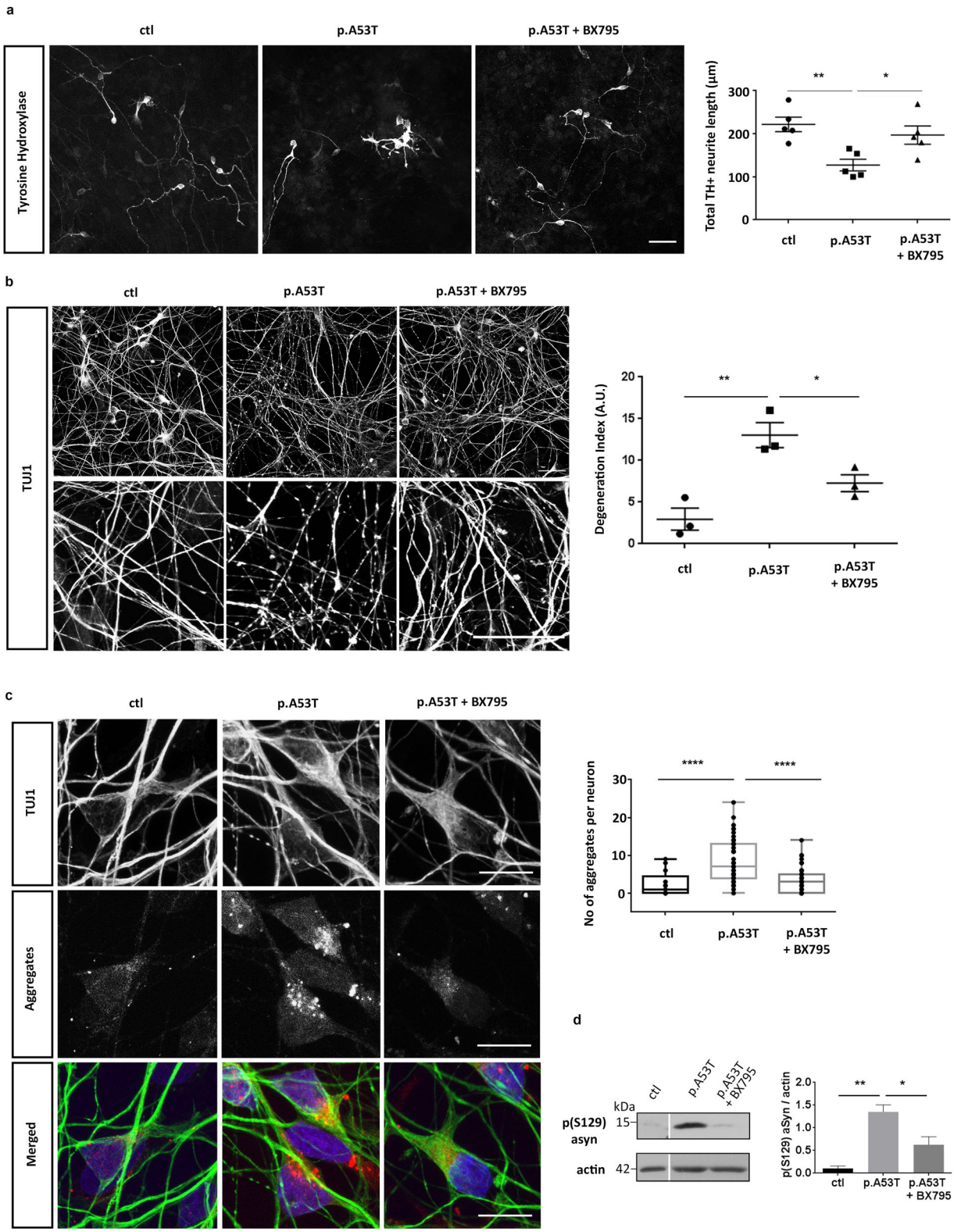

(Supplementary Fig. 5). Remarkably, the levels of a cohort of 118 proteins lying mostly within these biological processes and representing ~20% of the total dysregulated proteins in p.A53T neurons, were restored upon treatment with BX795 ($p < 0.05$) (Fig. 4a, Supplementary Table 3). Most important, this outcome was specific to p.A53T-neurons as BX795 had no significant effect on the proteome of control neurons (Supplementary Fig. 6)

Extensive data mining by GO enrichment analysis for biological processes, molecular function and cellular compartments ($p < 0.01$), complemented by reactome pathway analysis ($p < 0.01$), highlighted the dysregulated core pathways in p.A53T-neurons and, amongst them, those targeted by BX795 to restore neuronal physiology (Fig. 4b). These include proteins associated with RNA metabolism, protein synthesis, protein

Fig. 2 Rescue of neuropathological features in patient-derived p.A53T neurons by BX795. a BX795 has a positive effect on neurite length of p.A53T-neurons. Representative confocal images of healthy control (ctl) and p.A53T-neurons immunostained for TH and quantification of total neurite length of TH+ cells. Data represent mean ± SEM. (Comparisons by ANOVA with Tukey correction $^{*}P < 0.05$, $^{**}P < 0.01$, $n = 4$ independent experiments with at least 50 cells analyzed in each experiment). Scale bar, 50 μm. **b** BX795 alleviates axonal neuropathology in p.A53T-neurons. Higher magnification at the right (upper, DMSO-treated cells; lower, BX795-treated cells) shows neurites with swollen varicosities or fragmented processes (arrows). Scale bar, 30 μm. Quantification of axonal degeneration is estimated in the accompanying graph by measuring the ratio of TUJ1+ spots over the total TUJ1+ area in untreated (p.A53T) or BX795-treated p.A53T-neurons. Data represent mean ± SEM.(Comparisons by ANOVA with Tukey correction, $^{*}P < 0.05$, $^{**}P < 0.01$, $n = 20$ randomly selected fields for each condition; data was from three independent experiments). **c** BX795 reduces protein aggregates in p.A53T-neurons. Representative confocal images showing protein aggregates in p.A53T TUJ1+ neurons (Scale bar, 10μm) and quantification in untreated or BX795-treated TUJ1+ cells (Data was from three independent experiments. Mann–Whitney test; $n =$ at least 30 cells per group; $^{****}P < 0.0001$). **d** Detection and quantification of p(Ser129)αSyn by Western blot in control and p.A53T neurons in the absence or presence of BX795, as indicated; Actin shows equal protein loading. Data represent mean ± SEM (*t* test, $^{*}P < 0.05$, $n = 4$ independent experiments).

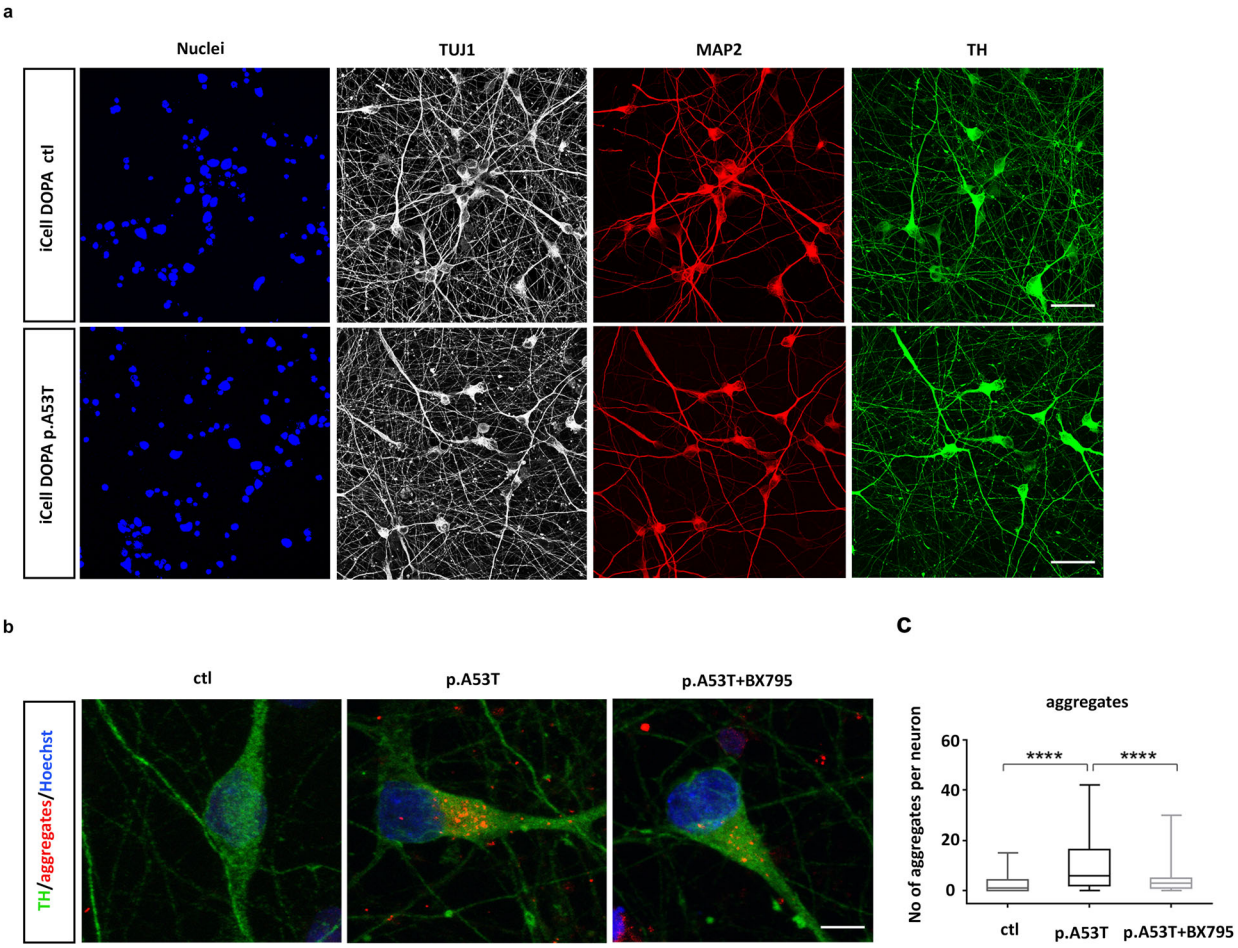

Fig. 3 BX795 reduces protein aggregates in a gene-edited p.A53T line of mature human iPSC-derived TH neurons. a Representative confocal images of wild-type (ctl) and isogenic p.A53T iCell Dopa neurons immunolabelled for Nuclei, TUJ1, MAP2 and TH. Scale bar, 30 μm. **b** Representative confocal images of wild-type (ctl) and isogenic p.A53T iCellDopa neurons showing immunostaining for tyrosine hydroxylase (TH green) and protein aggregates (red). p.A53T cells were treated or not with BX795, as indicated. Scale bar, 5 μm. **c** Quantification of aggregates in TH+ neurons. Data represent mean ± SEM. (Comparisons by ANOVA with Tukey correction, $^{****}P < 0.0001$, $n =$ at least 50 randomly selected TH+ cells for each condition).

modification and transport, stress response, and neurodegeneration, as outlined below.

RNA metabolism. The p.A53T proteome showed enrichment for proteins in subcellular compartments known to be associated with αSyn[38], including membrane bound organelles (204 proteins), mitochondria (118), ribosomal complexes (29), nucleus (292), and neuron projection/axon cytoplasm (10) (Supplementary Table 4). Processes such as cellular metabolism, translational initiation and regulation, tRNA aminoacetylation and export from nucleus, mRNA stability and export from nucleus, rRNA processing, formation of pre-initiation complex and protein folding were among the top pathways enriched in the p.A53T proteome (Supplementary Fig. 5). A previous study has identified mRNA binding proteins (RBPs) and those involved in protein biosynthesis within the protein network residing in immediate vicinity of αSyn, suggesting that perturbation of these pathways may be directly related to pathology[38]. Herein, we provide evidence that these

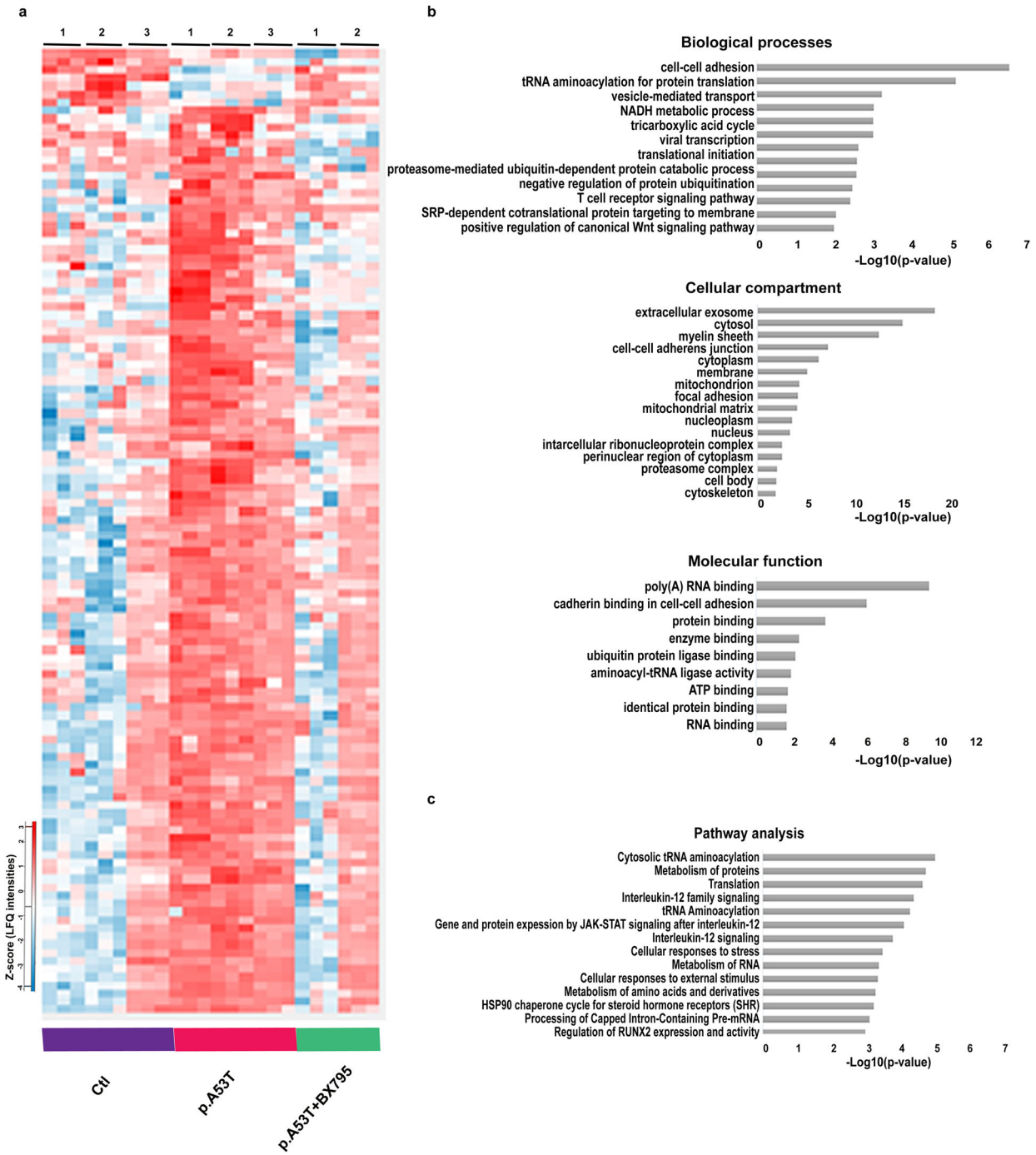

Fig. 4 Bioinformatics analysis of dysregulated proteins in p.A53T-neurons that are restored by BX795. a Hierarchical clustering of 118 upregulated proteins in patient-derived p.A53T-neurons that are restored upon treatment with BX795 (one-way ANOVA analysis). Columns in the different groups (control, p.A53T-neurons and p.A53T-neurons treated with BX795) correspond to individual samples tested and rows represent single proteins (blue, low expression; red, high expression; $n = 3$ for control and p.A53T; $n = 2$ for p.A53T + BX795). **b** GO enrichment analysis for biological processes, molecular function and cellular compartments was performed using DAVID software ($p < 0.01$). **c** Pathway analysis using Reactome software ($p < 0.01$).

same pathways are altered when p.A53T is expressed in human neurons (Supplementary Fig. 5). Specifically, a significant number of RBPs (60 proteins) were differentially expressed, including members with known neuronal localization and involvement in neuronal functions, such as ELAV-1, ELAV-3, RBBP7, RNPS1, RNMT, TARDBP, XPO1, XPO5, HNRNPA1, HNRNPA1L2, HNRNPF, HNRNPL, HNRPNPM, HRNNPUL1, PABPC1, PABPC4, PTBP2 and CELF1 (Supplementary Table 2). Since even small changes in RBP expression or activity are amplified due to their broad impact on expression, splicing and translation of numerous RNA substrates, changes in such a large number of these RNA regulators suggest a severe perturbation in RNA homeostasis in p.A53T-neurons. A cluster of RBPs implicated in splicing and adenylation events in the nuclear compartment (DEK, MYEF2, UBTF, SNRPB, PCBP1, ZNF207, HINT1, RAE1, HNRNPUL1) was restored after BX795 treatment (Fig. 5a).

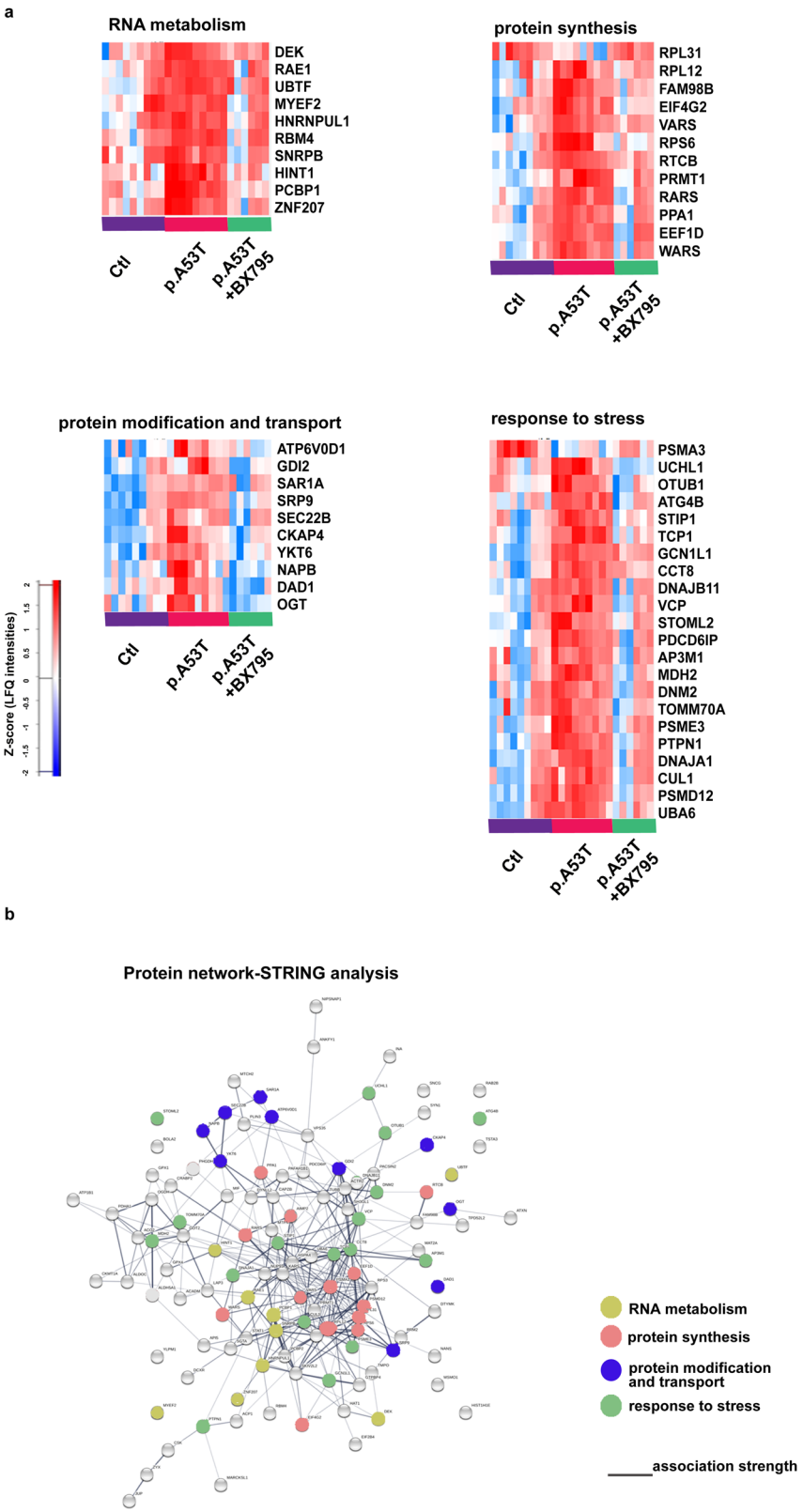

Fig. 5 Protein network of pathways and processes restored by BX795 treatment. a Heatmaps illustrating specific proteins upregulated in p.A53T-neurons that are involved in RNA metabolism, protein synthesis, protein modification and transport and response to stress, which are restored after BX795 treatment. High expression is in red and low expression is in blue. **b** STRING-analysis representation of the protein-protein interaction network of the 118 upregulated proteins in p.A53T-neurons that are restored by BX795. Each circular node depicts one protein and the different colors represent the different pathways/processes as indicated. Connecting lines represent protein-protein associations and line intensity represents the confidence score of a functional association.

Protein synthesis

Disturbances in RBP dosage have detrimental consequences also outside the nucleus, as they control the targeted localization of mRNAs, either proximally in the cell soma or distally in the projecting axon, affecting whether an mRNA will be translated or remain translationally silent and whether it will be stored for local mRNA translation or degraded[39]. Aberrant expression of the translational machinery emerged in the p.A53T proteome with translational initiation and regulation processes being the most affected in mutant neurons (Supplementary Fig. 5, Supplementary Table 2). A total of 18 proteins involved in the formation of the pre-initiation complex were identified and included EIF2, 3, 4 and 5, of which EIF4G2 that functions as a general suppressor of translation by forming translationally inactive stress granules, was affected by BX795 (Fig. 5a). Ribosomal proteins (29 proteins), structural components of ribosome subunits, were upregulated in p.A53T-neurons (Supplementary Table 2) and a significant fraction returned to near-control levels after BX795 treatment (Fig. 5a). These included RPL31 and RPL12, which are involved in 60 S biogenesis, and RPS6, a component of the 40 S subunit and downstream effector of the mTORC1 signaling pathway. tRNA processing represents another important part of the translational cascade that was altered in p.A53T-neurons (Supplementary Table 2), while a significant fraction was restored by BX795, including the aminoacyl-tRNA synthetases RARS (arginyl-tRNA synthase), VARS (valyl-tRNA synthase), and WARS (tryptophanyl-tRNA synthase) together with regulatory or accessory proteins such as PPA1, EEF1D PRMPT1, FAM98B and RTCB. Growing evidence associates changes in tRNA gene biogenesis and processing with neurodegenerative diseases[40]. Our data reveal for the a link between p.A53T-αSyn expression and this molecular process (Fig. 5a, Supplementary Table 2).

Protein modification and transport

p.A53T-αSyn toxicity has been attributed to problematic modifications at the ER membrane and disturbances in ER-Golgi and early endosomal/vesicle trafficking[33,38,41,42]. In accordance, p.A53T-neurons exhibit altered protein levels in components of these pathways (Supplementary Table 2). Among these, five members of the adaptor protein complexes that function in transport-vesicle mediated transfer between membranous structures are increased by p.A53T-expression (AP1B1, AP2A2, AP3B1, AP3D1 and AP3M1). Another prominent category included members of the largest branch of Ras-like small GTPases involved in membrane trafficking (RAB2A, RAB2B, RAB6B). In addition, proteins participating in ER to Golgi transport and macroautophagy (SEC22B, SEC31A, RAB18, ARF1, ARF3)[43,44], vesicle budding/uncoating in the Golgi apparatus (ARF1,ARF3)[45], SNARE-mediated autophagosome-lysosome fusion (RAB21)[46], retrograde Golgi to ER transport (COPA, COPB, COPG) (Supplementary Table 2) were also differentially expressed in p. A53T neurons.

BX795 had a selective effect on p.A53T-altered membrane transport proteins (SRP9, GDI2, ATP6VOD1, DAD1 subunit of oligosaccahryl transferase complex and OGT, and NAPB) and components of the SNARE complex (SAR1A, SEC22B and YKT6) (Fig. 5a) whilst alterations on molecules of the RAB, adaptor protein complex and coatomer remained largely unaffected.

Stress response

p.A53T-αSyn protein expression acts as a primary neurotoxin triggering a battery of stress responses in human neurons[47]. The proteomics analysis indicated that p.A53T neurons activate most of these mechanisms. Both the unfolded protein response (UPR), as evidenced by mis-expression of chaperones CCT2, 3, 4, 5, 7 and 8, as well as the heat shock protein response (HSP), with proteins such as DNAJA1, DNAJB11, DNAJC7, HSPA4L, HSP9 and HSPE1, were apparent in the p.A53T-proteome (Supplementary Table 2). These stress response pathways were significantly downregulated in p.A53T neurons treated with BX795, which seems to target many stress response mediators (Fig. 5a). These included TCP-1, a member of the chaperonin TCP1 complex (CCT), PTPN1, a UPR regulator, STIP1, a coordinator of HSP70 and HSP90 function and the chaperone/co-chaperone proteins DNAJB11, GCN1L1, CCT8, and DNAJA1.

Such a dysregulation of the UPR/HSP response systems in p. A53T neurons should result in the production of dangerous protein cargo and the formation of protein aggregates, as indeed identified by immunofluorescence (Fig. 2c). The p.A53T proteome also revealed alterations in protein clearance pathways with mediators of both proteasomal and autophagic systems being affected (Supplementary Table 2). BX795 improved the expression of multiple ubiquitin-associated proteins suggesting partial restoration of proteasome targeting of aberrant protein products, in accordance with the decrease of protein aggregates in BX795-treated p.A53T neurons (Fig. 2c). BX795 restored the expression of components of the proteasome complex and activators of the E2 and E3 ligase binding process (PSMA3, UCHL1, OTUB1, PSME3, CUL1, PSMD12, and UBA6), and VCP, an AAA ATPase that extracts ubiquitinated proteins from large protein complexes for degradation, previously shown to co-localize with protein aggregates in various neurodegenerative diseases (Fig. 5a).

Components of the lysosomal pathway of autophagy targeted by BX795 included vacuole transport components such as ATG4B and proteins required for multivesicular body (MVB) biogenesis and sorting (PDCD6IP, AP3M1 and DNM2) (Fig. 5a). Finally, BX795 also modulated oxidative stress response mechanisms, as the mitochondrial biosynthesis regulators TOMM70A and MDH2 were brought to near control levels. In addition, STOML2, a stimulator of cardiolipin biosynthesis recently shown to be associated with p. A53T neurotoxicity in human dopamine neurons was also positively targeted by BX795[33].

When STRING analysis was used to assess the relatedness level of all 118 proteins affected by BX795, a network with strong functional linkage among the majority of these proteins was revealed (Fig. 5b).

Proteins associated with neurodegeneration. An important measure of the biological significance of the proteomic profile of p. A53T neurons comes from comparisons with human genetic studies. Enrichment analysis for PD and other neurodegenerative diseases identified several proteins comprising both known and new converging targets that were modified by BX795 (Fig. 6a). Among those, UCHL1/PARK5 is linked to lower susceptibility for PD, while a point mutation co-segregating with the disease has been identified in one family[48] and VPS35/PARK17-D620N mutated protein causes late-onset autosomal dominant PD[49]. FAM98B has been linked to SMA and ALS[50], VCP mutations can cause FTD, ALS and Charcot-Marie-Tooth diseases[51,52], HINT1 autosomal recessive mutations lead to neuromytotonia and axonal neuropathy[53], PAFAHB1 mutations and gene deletions lead to lissencephaly syndrome[54] and RBM4 is linked to Down's syndrome[55] (Fig. 6a, b). STRING analysis of the BX795-modified protein network to which αSyn was also incorporated, demonstrated a strong association between αSyn and two other neurodegeneration-linked proteins (Fig. 6c).

These findings deepen our understanding of p.A53T-mediated neurotoxicity and reveal key biological processes that are targeted by BX795 to alleviate p.A53T-αSyn-related phenotypes in human neurons.

BX795 affects the mTORC1 signaling pathway to attenuate protein synthesis and facilitate autophagic flux in p.A53T neurons

The p.A53T proteome clearly indicates aberrant mRNA translation and protein clearance mechanisms, both linked to mammalian aging

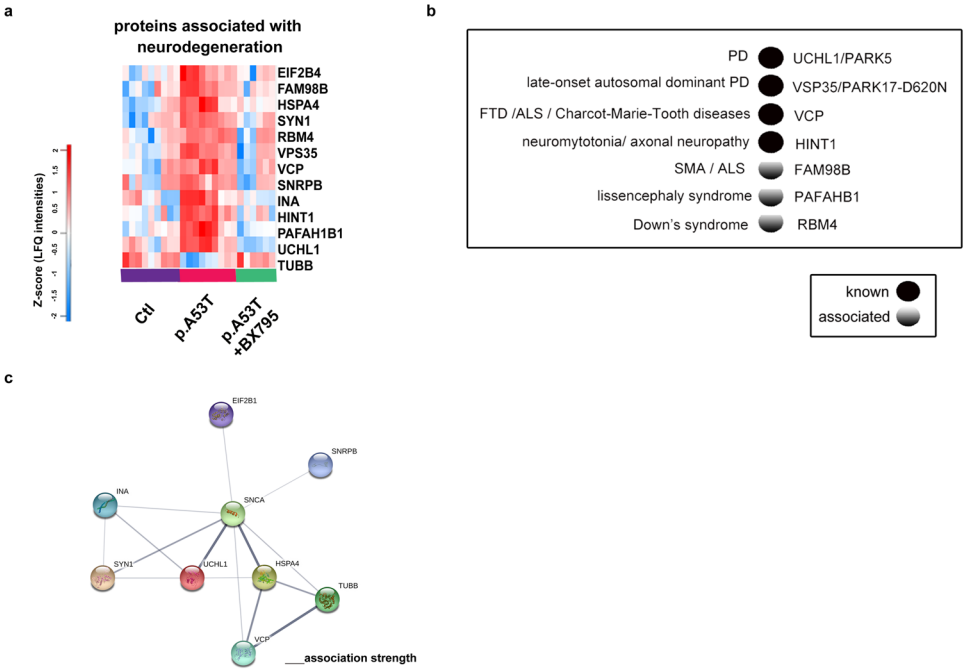

Fig. 6 Restoration of disease-associated proteins by BX795 in p.A53T-neurons. a Heatmap of proteins associated with neurodegeneration that are restored after BX795 treatment. High expression is in red and low expression is in blue. **b** Disease-associated proteins that are modified by BX795 are either known or associated genetic risk factors for neurodegenerative diseases as revealed by human genetic studies. **c** STRING network analysis of the neurodegeneration-associated proteins restored by BX795 in p.A53T-neurons and their interaction with αSyn. Each αSyn interactor is shown as a colored circle and connecting lines between proteins represent protein-protein associations. The intensity of lines represents the confidence score of a functional association.

and neurodegenerative diseases that can be effectively restored by BX795. The mammalian target of rapamycin (mTOR) signaling pathway is a central regulator of proteostasis and the p.A53T proteome clearly indicates hyperfunctional overactive biosynthetic processes that could be associated with alterations in mTORC1 activation. Components of this signaling cascade have emerged in the proteomics analysis of p.A53T- neurons, including RPS6, a major downstream effector of mTORC1, together with several RAG GTPases like IQGAP1, required for efficient activation of mTORC1, which were largely restored after BX795 treatment (Supplementary Table 3). To validate the activation of the mTORC1 pathway in p.A53T patient-derived neurons, we examined the levels of phosphorylated RPS6 (pRPS6), which is commonly used as a readout for mTOR signaling. Indeed, we observed significantly higher levels of pRPS6 in p.A53T neurons as compared to control that were efficiently downregulated upon BX795 treatment (Fig. 7a, b).

To confirm that the p.A53T mutation is causally related to dysregulation of protein metabolism and verify that BX795 can restore this effect in mature human neurons, we exploited the isogenic system of iCell DopaNeurons where we measured the levels of the activated form of RPS6, and the total protein synthesis rate. The presence of the p.A53T mutation led to a significant increase in the levels of pRPS6 (Fig. 7c, d) that correlated with a significant increase of global protein synthesis in iCell Dopa p.A53T neurons (Fig. 7c, d). BX795 could lower significantly the levels of pRPS6 and reverse the aberrantly increased protein synthesis rate (Fig. 7c, d). This data suggests that BX795 targets and restores dysregulated mRNA translation and protein synthesis pathways instigated by the p.A53T mutation in neuronal cells.

To examine further the effect of the p.A53T mutation on mTORC1 activity and protein synthesis, we created stably transduced SH-SY5Y neuroblastoma cells co-expressing the human p.A53T-αSyn and the fluorescent protein DsRed or DsRed only as a control (Fig. 8a). Upon neuronal differentiation, SH-SY5Y cells expressing the human p.A53T-αSyn displayed a prominent upregulation in the levels of phosphorylated mTOR and pRPS6 as compared to control cells (Fig. 8b), whilst BX795 had an acute effect in downregulating their levels (Fig. 8c), as determined by Western blot analysis.

Biochemical and genetic studies have identified the upstream p70 S6 kinase as the main in vivo kinase responsible for RPS6 phosphorylation[56]. Since a most prominent observation in all p.A53T-bearing cells tested in our study was an up-regulation of pRPS6 and its downregulation by BX795, we asked if the compound could inhibit the activity of p70 S6 kinase. To this end, we assessed the kinase activity of purified recombinant p70 S6K in the absence or presence of BX795 and found a notable dose-dependent inhibitory effect (Fig. 8d), indicating that BX795 may restore pRPS6 levels and protein synthesis by targeting p70 S6K. Finally, we checked if MHY-1485, a synthetic mTOR activator, could counteract the beneficial effects of BX795 in p.A53T cells. Consistently, upon co-treatment with MHY-1485 and BX795, we could not see a reduction in pathological p129S-αSyn levels in SH-SY5Y cells expressing human p.A53T-αSyn or a decrease in neuronal aggregates in p.A53T iPSC-derived neurons (Fig. 8e, f).

mTORC1 also controls autophagy, the major degradation pathway essential for removing aggregation-prone αSyn[57,58]. To test if BX795 could also affect this clearance pathway, we utilized a previously established inducible SH-SY5Y cell line that expresses the human p.A53T-αSyn upon withdrawal of Doxycycline (-Dox). In this model, expression of mutant p.A53T has been shown to cause perturbation of the autophagy lysosomal pathway resulting in increased steady-state levels of LC3II and p62[59]; (Fig. 9 a, b). p62 is a receptor for ubiquitinated cargo destined to be degraded by autophagy and is associated with LC3-II, the processed form of LC3, within autophagosomes and autolysosomes[60,61]. To visualize LC3-II and quantify GFP-LC3-II+ puncta comprising brightly fluorescent autophagosomes and more weakly labeled autolysosomes (Fig. 9a), we transfected the inducible SH-SY5Y line with a fusion construct containing the green fluorescent protein tagged to LC3 (GFP-LC3)[62].

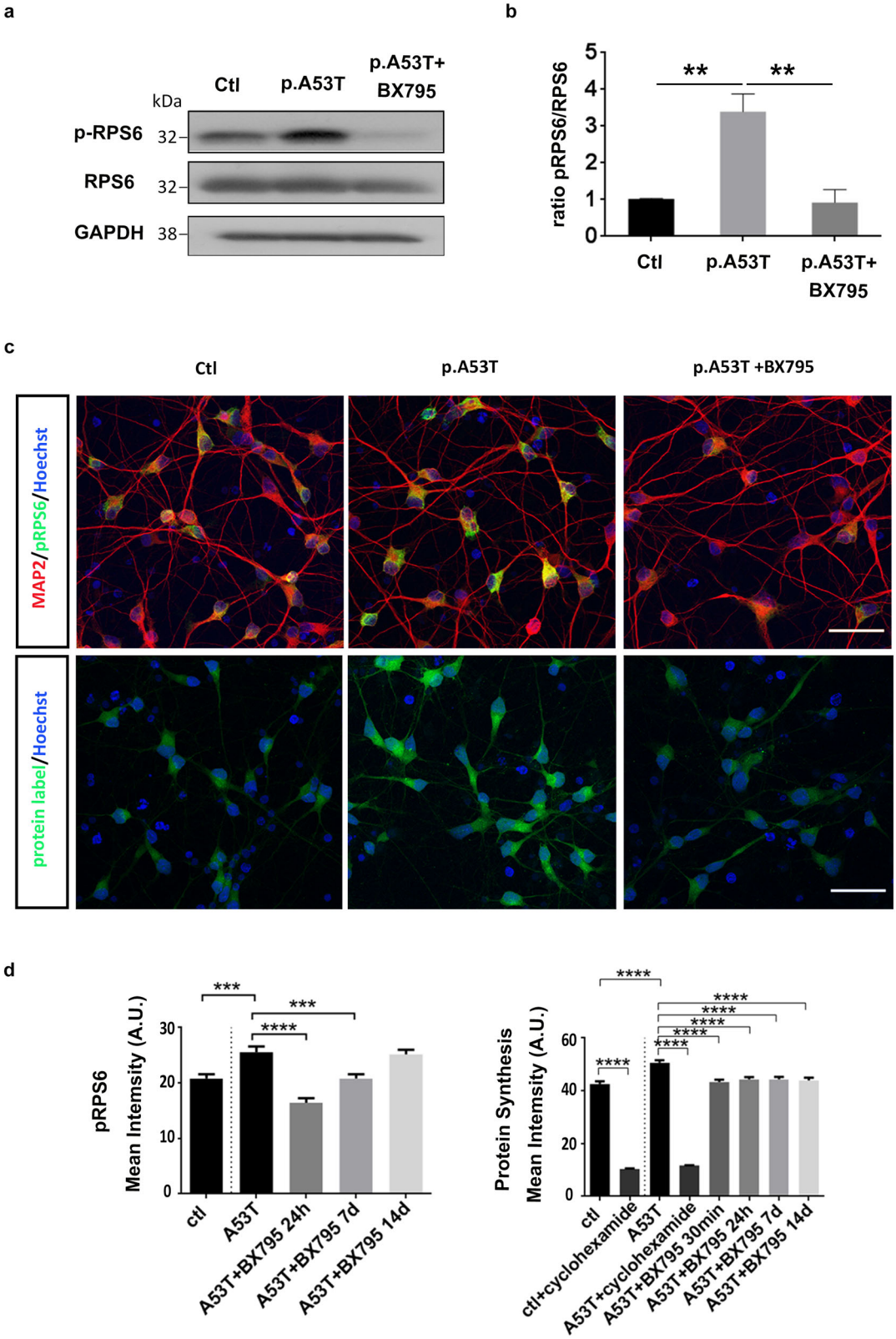

In agreement with the Western blot data, GFP-LC3-II+ puncta were scarce in p.A53T cells treated with DMSO while in the presence of BX795 there was a small, yet not significant increase (Fig. 9c, d). As expected, when DMSO-treated cells were exposed to bafilomycin, a blocker of autophagosome-lysosome fusion that prevents lysosome-mediated protein degradation, GFP-LC3-II+ puncta increased significantly (Fig. 9c, d)., Addition of both bafilomycin and BX795 further increased the number and brightness of GFP-LC3-II+ puncta, suggesting that BX795 acts as an autophagy inducer (Fig. 9c, d).

Fig. 7 BX795 affects the mTORC1 signaling pathway in p.A53T patient-derived and iCell Dopa neurons to attenuate protein synthesis. **a** Western blot showing increased levels of p-RPS6 in p.A53T-patient iPSC-derived neurons and a notable reduction in the presence of BX795. GADPH shows equal protein. **b** Quantification of p-RPS6 levels in p.A53T-patient iPS-derived neurons. Data represent mean ± SEM (Comparisons by ANOVA with Bonferroni's multiple comparisons test. $^{**}P < 0.01$, $n = 3$ independent experiments). **c** Representative confocal images of control (ctl) and isogenic gene-edited p.A53T iCellDopa neurons, either non-treated or treated with BX795. Cells were immunolabeled for phosphorylated RPS6 (green) andmicrotubule associated protein 2 (MAP2; red)(upper panel) and labeled for total protein synthesis (protein label, green)(lower panel). Nuclei are seen with Hoechst dye (blue). Scale bar, 30 μm. **d** BX795 reduces phosphorylated RPS6 levels and reduces total protein synthesis in p.A53T-neurons. Quantification of fluorescence intensity in control, untreated p.A53T or BX795-treated p.A53T neurons. Data represent mean ± SEM (Comparisons by ANOVA with Tukey correction, $^{***}P < 0.001$ $^{****}P < 0.0001$, $n = 100$ randomly selected cells for each condition).

To distinguish labeled autophagosomes from autolysosomes and monitor the autophagic flux, we used a dual fluorophore probe consisting of a tandem fluorescent mCherry-GFP-p62 construct[63]. GFP fluorescence is sensitive to low-pH and labels only neutral-pH autophagosomes, while mCherry retains fluorescence in both autophagosomes and low-pH autolysosomes[61] (Fig. 9e). Calculation of the ratio of GFP+ /mCherry+ puncta presents a measure of the autophagic flux, and a reduction in this ratio mirrors an increase in the progress of autophagy. Indeed, quantification of green and red puncta revealed a significantly lower GFP/mCherry ratio in the presence of BX795 as compared to DMSO-treated cells, indicating that BX795 facilitates the the autophagic flux (Fig. 9f, g). In agreement, a decrease in the total levels of p62 was noted upon treatment with BX95 (Fig. 9h).

Last, we examined if BX795 had a similar effect in facilitating autophagic flux in p.A53T patient-derived neurons. Electron microscopy observations revealed that these cells have prominent autophagosomes exemplified by multi-lamellar vacuoles that were never detected in control cells (Fig. 9i). These findings are consistent with an accumulation of autophagosomes resulting from stalled autophagic flux in p.A53T cells. To assess the effect of BX795, we used the Cyto-ID® autophagy detection kit that monitors autophagosomes and autophagic flux using a using a dye that selectively labels accumulated autophagic vacuoles by fluorescence microscopy. As expected, p.A53T neurons showed an accumulation of fluorescent autophagosomes that were effectively decreased upon BX795 treatment, indicative of restoration of autophagic flux (Fig. 9j).

Overall, our results indicate that BX795 can restore proteostasis in p.A53T cells by modulating aberrant protein synthesis and facilitating protein clearance mechanisms.

DISCUSSION

The generation of human models based on patient-derived iPSCs has opened up new perspectives for investigation of disease mechanisms and discovery of new therapeutics. In this work, we used a well-characterized human model of p.A53T pathology[22] to screen for small molecules with protective function. We identified the multi-kinase inhibitor BX795 as a compound that exerts a consistent and sustainable beneficial effect on patient-derived p.A53T-neurons. Remarkably, we found that a single treatment with BX795 has long-lasting consequences in supporting neuritic growth, limiting αSyn protein aggregate formation and restoring axonal neuropathology, recorded two weeks after its addition in human p.A53T neurons.

This study represents a high-content drug discovery screen performed in human p.A53T iPSC-derived neurons to identify candidate therapeutics for PD. Using an unbiased screening approach in combination with quantitative proteomics profiling, we were able to show that treatment with BX795 restored proteins associated with key cellular processes, most notably RNA metabolism, protein synthesis and degradation processes, as well as stress response, suggesting that restoration of proteostasis is key for rescuing the neuropathological features in p.A53T-neurons. Dissecting further the pathways affected by BX795, we demonstrated that BX795 modulates the mTORC1 pathway to restrict excessive protein synthesis and facilitate autophagy. Taken together, our data highlight the BX795 kinase inhibitor as a promising compound and candidate therapeutic that ameliorates p.A53T-associated pathology. Moreover, our results show that interfering with and restoring proteostasis downstream mTOR signaling can have long-term beneficial consequences in cellular health by instigating constitutive changes.

Considerable progress in understanding the neurotoxic properties of α-Syn has been achieved by exploiting causal mutations resulting in rare familial forms of PD, most notably the p.A53T-αSyn mutation (G209A in the *SNCA* gene)[64,65]. We and others have shown that disease-associated characteristics can be recapitulated in patient-derived p.A53T-neurons, including axonal degeneration and accumulation of protein inclusions resembling Lewy bodies and neurites[22]. These have been linked to multiple molecular defects in mRNA processing and translation, endocytic and retrograde trafficking[38,42], protein misfolding, redox homeostasis[20,33] and the synaptic protein machinery[22]. The p.A53T proteome examined here revealed a profound increase in proteins related to the biological processes of RNA metabolism, protein synthesis, modification and transport, protein clearance and stress response. Notably, the cohort of 118 proteins that was specifically restored in p.A53T-neurons upon treatment with BX795, was associated with these key cellular processes.

The pathways affected by mutant αSyn in our study have a high similarity with the αSyn connectome reported by Chung et al.[38] for mouse neurons, and the predictions of the in silico "humanized" map of αSyn proteotoxicity reported in the accompanying study of Khurana et al.[42]. Our proteomics analysis, accomplished in p.A53T-human neurons, identified perturbations in RNA metabolic processes that started from the nucleus and reached the ribosome. Alternative mRNA processing greatly increases the dimensions of gene expression through splicing, polyadenylation, targeted localization and post-transcriptional silencing. Neurons take advantage of all these strategies as the brain has the highest levels of alternative splicing compared to any other human tissue[66]. This process has recently been shown to be defective in the PS19 Tau model of Alzheimer's disease, where alternative splicing events affected genes particularly involved in synaptic transmission[67]. Similarly, the p.A53T-proteome suggests that this process could be excessively induced in p.A53T-neurons as a number of RBPs known to be linked to αSyn aggregation have emerged, including ELAV1, ELAV3 and CELF, suggesting a possible association with the abnormal expression of synaptic genes and the defective synaptic connectivity we have previously reported in p.A53T neurons-[22].

An excess of mRNAs coming out of the nucleus in p.A53T-neurons could explain the abnormal expression of proteins involved in translation, the next step of mRNA processing. The significant increase of components of the tRNA splicing ligase complex, various aminoacyl-tRNA synthetases, ribosomal subunits and eukaryotic translation initiation factors indicate an enhanced translation of spliced mRNAs. Moreover, in post-mortem PD brains, region and stage-dependent alterations in the machinery of protein synthesis have been reported and have been associated with α-synuclein oligomers in remaining neurons[68].

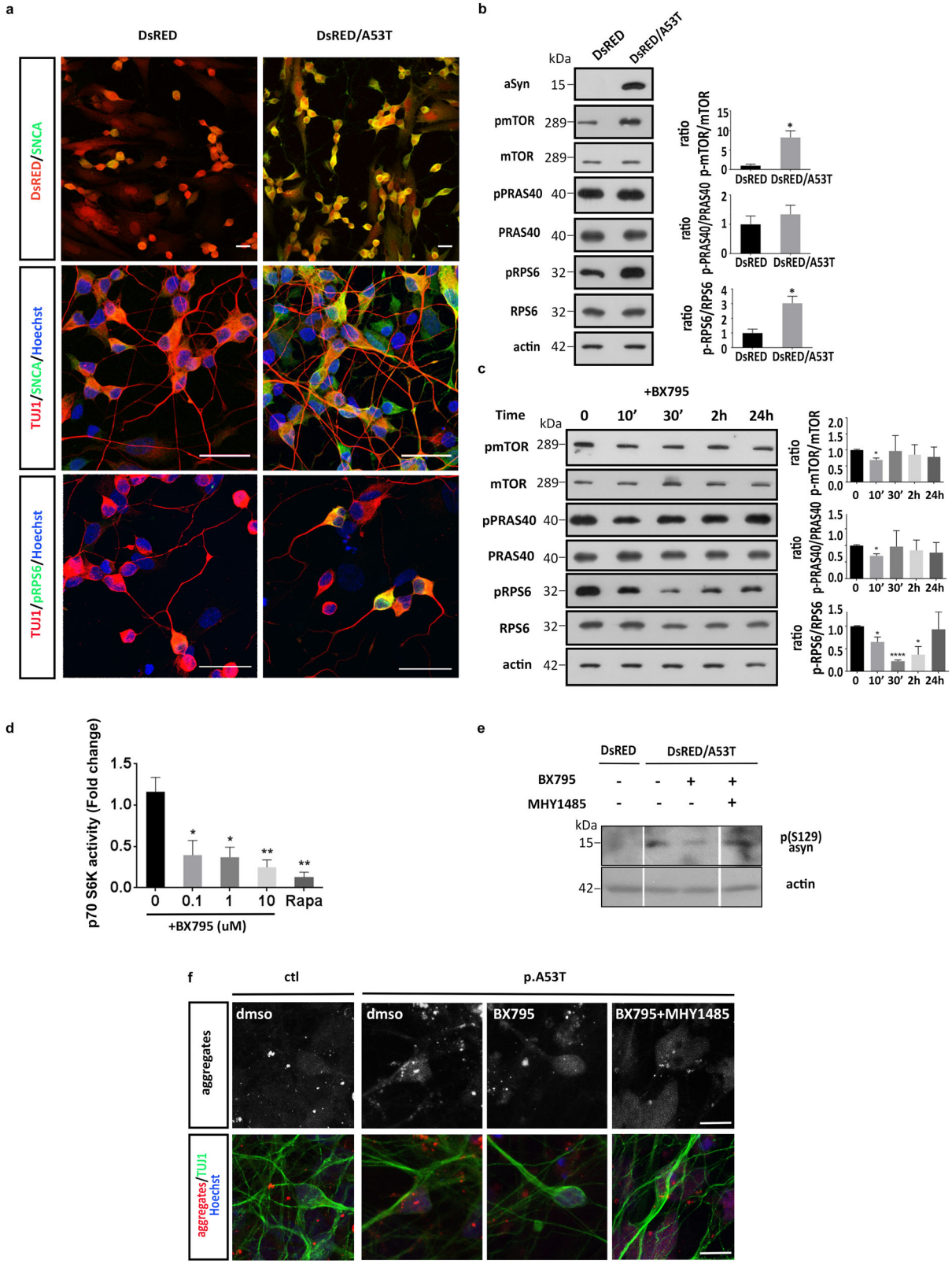

The mTOR kinase is a master regulator of cellular metabolism that functions in two distinct complexes: mTORC1 and mTORC2[69] with the first implicated in protein and lipid biosynthesis through a signaling cascade that includes SK6 and 4E-BP1 proteins[70]. Unlike proliferating cells where this pathway is utilized for growth and division, in neurons it acts as a regulator of healthy metabolism and aging[71] with its restriction being associated with prolonged life span and delay of age-related pathologies. p.A53T neurons have increased RPS6, IQGAP1 and RAG-GTPases, components of mTORC1 pathway and this seems to be associated with

Fig. 8 BX795 restores neurodegenerative phenotypes via the mTORC1 signaling pathway. a Representative images of SH-SY5Y cells stably transduced to express DsRed only or DsRed and human pA53T-αSyn. After neuronal differentiation, cells were immunolabled for αSyn (SNCA), TUJ1 and pRPS6. **b** Western blot showing that the presence of mutant SNCA in differentiated p.A53T-transduced SH-SY5Y cells, results in an increase in the levels p-mTOR and p-RPS6. Actin shows equal protein loading. Data represent mean ± SEM (*t* test, $^{*}P < 0.05$, $n = 3$ independent experiments). **c** Western blot showing an acute reduction in the levels of p-mTOR and p-RPS6 in the above stably transduced and differentiated SH-SY5Y cells, in the presence of BX795. Actin shows equal protein loading. Data represent mean ± SEM (Comparisons by ANOVA with Tukey correction, $^{*}P < 0.05$, $^{****}P < 0.0001$, $n = 3$ independent experiments). **d** BX795 inhibits the kinase activity of pure recombinant p70 S6K (25 ng/assay) in a dosedependent manner. Rapamycin (Rapa) was used as a positive control. Data represent mean ± SEM (Comparisons by ANOVA with Tukey correction, $^{*}P < 0.05$, $^{**}P < 0.01$, $n = 3$). **e** Western blot showing the effect of BX795 treatment alone and in combination with mTOR activator MHY-1485 on the p(Ser129)-αSyn levels in SH-SY5Y cells stably transduced to express DsRed only or DsRed and human pA53T-αSyn. **f** Representative confocal images show protein aggregates in control (ctl) and patient p.A53T neurons, either non-treated (DMSO) or treated with BX795 alone or in combination with the mTOR activator MHY-1485.

an increased translation of a subset of mRNAs that are linked to RNA metabolism and the stress response. Similarly, a quantitative proteomics study of a pre-symptomatic p.A53T-αSyn Drosophila model shows significant upregulation of ribosomal proteins in the p.A53T flies[72]. Although the mechanistic link between p.A53T-αSyn and mTORC1 remains to be established, recent evidence shows that genetic variability in the mTOR pathway contributes to SNCA effects in disease pathogenesis[73].

Concomitantly with promoting protein synthesis mTORC1 acts to repress autophagy through ULK1 phosphorylation. Autophagy has a central role in promoting health and longevity while this process is impaired in neurodegenerative diseases and αSyn pathology[74,75]. The p.A53T-proteome shows that neurons are under stress as proteins involved in the UPR or the heat-shock stress response, proteasome assembly and regulation, known to be orchestrated by mTORC1 in neurons, are significantly upregulated[71]. Restoration of numerous components of RNA metabolism and protein translation cascades by BX795 is directly related to the diminished stress response that emerges by the lower levels of UPR and heat-shock-associated proteins also conferred by this molecule. In parallel, a significant number of ubiquitin/proteasome-associated proteins were brought back to near control levels suggesting that BX795 helps misfolded protein clearance by limiting protein synthesis. This is in agreement with its demonstrated ability to decrease protein aggregates in p.A53T-neurons, as shown in this study, along with facilitation of autophagy both in SYSH-5Y cells expressing p.A53T and in patient-derived neurons.

BX795 is a multi-kinase inhibitor that targets numerous pathways, including the kinases TBK1 and PDK1[29–31,35]. Although in our system differences in the total or phosphorylated levels of these two kinases were not observed in the presence of BX795 (data not shown), we cannot exclude that its effects are mediated through these two kinases as both are involved in neurodegeneration, mTOR signaling and autophagy[76,77]. Yet four other PDK1 inhibitors that were included in the Selleck library did not emerge as hits during the screening campaign. Interestingly, we found that BX795 could inhibit purified recombinant p70 S6K, the major kinase that phosphorylates RPS6 in vivo, indicating that the acute effect of the compound on RPS6 in p.A53T-expressing cells could be mediated through inhibition of p70 S6K. It is notable that multiple other inhibitors of mTOR phosphorylation present in the kinase inhibitor library tested (26 in total, including rapamycin), failed to show any protective effects. Considering that BX795 has been proposed to act through distinct mechanisms in different pathologies, future mechanistic studies should reveal its direct targets in p.A53T neurons. Nevertheless, the work presented here uniquely identifies BX795 as a promising compound that may have therapeutic potential for patients with PD and other protein conformational disorders. Further, our collective data along with previous proteomics and systems approaches shed light into the molecular and cellular pathways of αSyn proteotoxicity unveiling new disease targets for the development of combined therapeutics.

METHODS

Directed neuronal differentiation

iPSCs used in this study were previously generated and characterized from two Parkinson's disease patients harboring the p.A53T-α-synuclein mutation and a healthy subject (control, wild-type SNCA)[22]. For directed differentiation, iPSCs were allowed to form embryoid bodies and neural induction was initiated by applying a dual SMAD inhibition protocol in the presence of Noggin and TGFβ inhibitor for generation of neural precursor cells (NPCs)[22]. NPCs were expanded in DMEM/F12/B27/N2-medium supplemented with HEPES, Glutamax, non-essential amino acids [NEAA] and 20ug/ml FGF2. For neuronal differentiation, NPCs were dissociated with accutase and seeded onto poly-L-ornithine (20 µg/ml; Sigma-Aldrich)/ laminin (5 µg/ml; Sigma-Aldrich)-coated dishes in DMEM/F12/ B27/N2-medium supplemented with 200 ng/ml human recombinant sonic hedgehog (SHH, R&D Systems) and 100 ng/ml murine recombinant fibroblast growth factor 8b (FGF-8b, R&D Systems) for 7 days in vitro (DIV). Cells were then replated in medium supplemented with 20 ng/ml brain-derived neurotrophic factor (BDNF, R&D Systems), 20 ng/ml glial cell-derived neurotrophic factor (GDNF, R&D Systems), 200 µM ascorbic acid (AA, Sigma-Aldrich) and 0.5 mM cyclic AMP (cAMP, Sigma- Aldrich). The medium was changed every 2 to 3 days for 2 weeks.

iCell Dopa neurons and isogenic iCell DopaNeurons PD SNCA A53T HZ

Commercially available iCell DopaNeurons 01279, Catalog No C1028, and a heterozygous (HZ) A53T allelic variant isogenic to iCell DopaNeurons, PD SNCA A53T HZ 01279, Catalog No C1113, in which the site-specific p.A53T mutation was introduced into the *SNCA* gene by nuclease-mediated SNP alteration, were purchased from Fujifilm Cellular Dynamics International and were maintained according to the User's Guide protocol for two weeks unless otherwise stated.

Compound screening and High Content image analysis

iPSC-derived NPCs at 7 DIV were dissociated with accutase, seeded (9,000 cells/well) onto poly-L-ornithine/ laminin-coated 384-well optical bottom plates containing the kinase inhibitors (Greiner Bio-One, Kremsmünster, Austria) and cultured in neuronal differentiation medium for two weeks (Fig. 1a). A collection of 273 small molecule kinase inhibitors from Selleck Chemicals was used. The list of inhibitors and their known targets according to the provider, is shown in Supplementary Table 1. The compounds were dispensed in duplicate in 384-well optical bottom plates at a final concentration of 1 µM, followed by NPC seeding. After 2 weeks of neuronal differentiation, cells were fixed in 4% paraformaldehyde for 20 min followed by immunofluorescence for βIII-tubulin (TUJ1) and Tyrosine hydroxylase (TH) at 4 °C overnight and incubation with appropriate secondary antibodies (Molecular Probes, Thermo Fisher Scientific) conjugated to AlexaFluor 488 (green) or 546 (red), for at least 1 h at room temperature. Nuclei were stained with Hoechst dye. Images were captured by automated confocal microscopy (Opera High-Content Screening System, Perkin Elmer, Hamburg, Germany). A total of 15 images per well were acquired using a 10X magnifying objective. Cell nuclei and fluorescence staining were quantified by segmentation on 15 images per well in a duplicate experimental setup. Parameters were set as follows: primary object detection (cell nuclei) was based on Hoechst staining, captured in channel 1. Detection of neurons was based on TUJ1 immunofluorescence signal, captured in channel 2 and on TH immunofluorescence

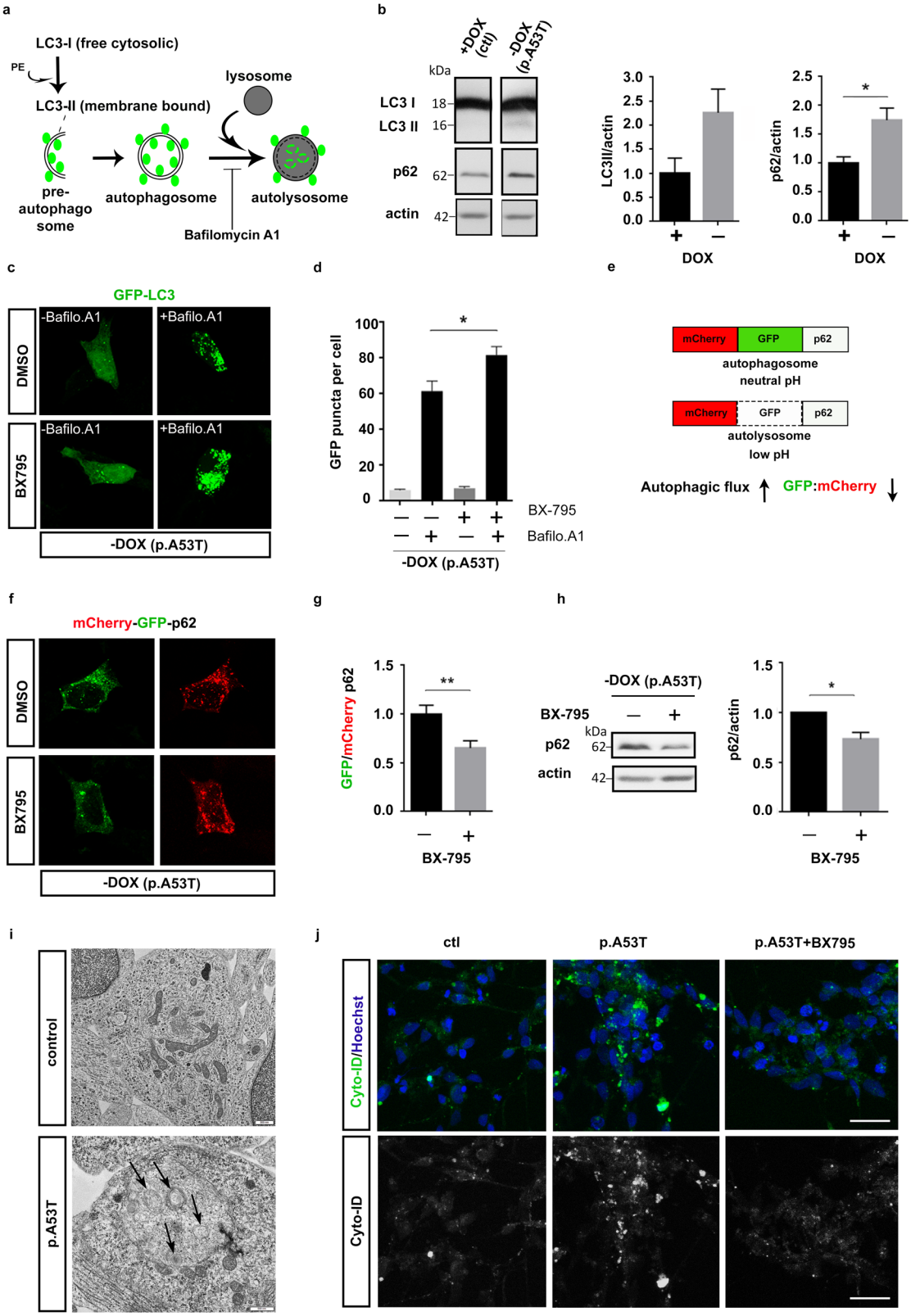

signal, captured in channel 3. For quantification of TUJ1 and TH intensity Image Mining was used, a custom-made image processing and analysis application with an extendable "plug-in" infrastructure[78]. DMSO was used as negative control at the same concentration as in the compound library. Hit compounds were selected using the following criteria: (1) all molecules that decreased the cell number within a well by more than 30% were considered toxic and were discarded; (2) compounds with a mean intensity ratio of TH vs TUJ1 outside two standard deviations of the negative DMSO control were selected as positive.

RNA isolation, cDNA Synthesis and qRT-PCR

Total RNA was extracted from cell pellets using the TRIzol® Reagent (Life Technologies). Following digestion with DNaseI, 1 µg of total RNA was used

Fig. 9 BX795 facilitates autophagy in an inducible SH-SY5Y cell line expressing human p.A53T-αSyn. a Schema illustrating that cytosolic LC3 is cleaved to yield LC3-I, which is subsequently conjugated to phosphatidylethanolamine (PE) to form membrane-bound LC3-II (green circles). Pre-autophagosomal structures engulfing protein cargo and organelles destined for degradation close to form double membrane spherical autophagosomes. These fuse with lysosomes to yield autolysosomes and their contents are degraded. Bafilomycin blocks autophagic flux by inhibiting autophagosome-lysosome fusion, which results in accumulation of LC3-II+ autophagosomes. **b** Representative immunoblot showing steady-state levels of LC3-II and p62 in lysates of inducible SH-SY5Y cells expressing the human p.A53T-αSyn (-Dox) and quantification relative to actin. Data represent mean ± SEM, *t* est, $*P < 0.05$, $n = 3$ independent experiments. **c** Representative confocal images of individual p.A53T SH-SY5Y cells (-Dox) transfected with GFP-LC3 that were treated or not with bafilomycin A1 in the absence or presence of BX795. **d** Quantification of GFP-LC3 puncta per cell. Comparisons by ANOVA with Tukey correction. $*P < 0.05$, $n = 72$ cells (control DMSO), $n = 79$ cells (BX795), $n = 67$ cells (Bafilomycin A1), $n = 68$ cells BX795 + Bafilomycin A1. Data are representative of three independent experiments). **e** Assessment of autophagic flux using mCherry-GFP-LC3 color change between autophagosomes and autolysosomes. Autophagic flux is induced when the GFP:mCherry ratio is reduced. f, g. Representative confocal images of individual cells [inducible SH-SY5Y cell line expressing p.A53T-αSyn (-Dox)] transfected with GFP-mCherry-p62 that were treated with DMSO (control) or BX795 and quantification of the ratio of GFP +/mCherry+ puncta (*t* test, $n = 60$ (control DMSO), $n = 53$ (BX795) $**P < 0.01$ Data are representative of three independent experiments). **h** Representative immunoblot showing steady-state levels of p62 in cells [inducible SH-SY5Y cell line expressing p.A53T-αSyn (-Dox)] treated or not with BX795, and quantification relative to actin. Data represent mean ± SEM, *t* test, $n = 3$ independent experiments. **i** Representative electron micrographs showing control and patient-derived p.A53T cells. Multilamellar autophagic vacuoles (arrows) are depicted in p. A53T cells; in this case they seem to be engulfed by an additional membranous structure. Scale bar 500 nm. **j** Representative confocal images showing autophagosome accumulation (brightly labeled green spheroids) in patient-derived p.A53T neurons as compared to either control (ctl) or p.A53T cells treated with BX795. Scale bar, 30 μm.

for first strand cDNA synthesis with the ImProm-II Reverse Transcription System (Promega) according to the manufacturer's instructions. Quantitative RT-PCR analyses were carried out in a Light Cycler 96 (Roche) real time PCR detection system using KAPA SYBR FAST qPCR Master Mix (KapaBiosystems). All primers used are listed in Supplementary Table 5.

Immunofluorescence staining

Cells were paraformaldehyde-fixed, blocked with 5% donkey serum in PBS/0.1% Triton X-100 (Sigma-Aldrich) for 30 min and immunofluorescence labeled as above. Coverslips were mounted with ProLong Gold antifade reagent with DAPI (Cell Signaling) and images were acquired using a Leica TCS SP8 confocal microscope (LEICA Microsystems) and analyzed using ImageJ software (NIH). All primary antibodies used are listed in Supplementary Table 6.

Neurite analysis

Neurite length was estimated manually by tracing the length of all neurites on TH-labeled neurons at 21 DIV using the NeuronJ plugin of ImageJ (NIH). At least 50 single TH+ neurons per sample were analyzed.

Axon degeneration index

The number of TUJ1+ spots in blebbed or fragmented axons was counted manually (ImageJ) on twenty randomly selected fields and the ratio between the number of spots and the total TUJ1+ staining area (ImageJ) was defined as axon degeneration index [22].

Protein aggregate quantification

Protein aggregates were detected with the PROTEOSTAT Aggresome Detection Kit (Enzo) followed by immunolabeling for TUJ1 or TH[22,32]. Manual analysis was performed by isolating individual cells from images (ROIs), applying a threshold, and utilizing the 'analyze particles' ImageJ function.

Proteomic analysis

The same line of patient-derived neurons used for high content screening was used for proteomics analysis vis-à-vis a healthy control. At 21 DIV iPSC-derived neurons were suspended, lysed and the proteins reduced in 4% SDS, 100 mM DTT, 100 mM Tris pH 7.8 through heating for 5 min. Next, the proteins were alkylated by 100 mM iodoacetamide treatment for 30 min in the dark. Samples were further processed according to the Single-Pot Solid-Phase enhanced Sample Preparation (SP3) method of Hughes et al.[79]. Digestion was carried out overnight at 37 °C using Trypsin/LysC mix (Promega) at a protein/enzyme ratio of 50:1 in a ThermoMixer under continuous mixing at 1000 rpm. After digestion, the tubes were placed on a magnetic rack, and the supernatant containing the peptides was collected and dried down in a centrifugal evaporator (Savant SPD 1010, Thermo scientific). The peptide mixtures were reconstituted in a solution of 2% (v/v) ACN/ 0.1% (v/v) formic acid and incubated for 3 min in a sonication water bath. Peptide concentration was determined by nanodrop absorbance measurement at 280 nm.

Ultra-high pressure nanoLC

2.5 μg peptides were pre-concentrated with a flow of 3 μL/min for 10 min using a C18 trap column (Acclaim PepMap100, 100 μm × 2 cm, Thermo Scientific) and then loaded onto a 50 cm long C18 column (75 μm ID, particle size 2 μm, 100 Å, Acclaim PepMap100 RSLC, Thermo Scientific). The binary pumps of the HPLC (RSLCnano, Thermo Scientific) consisted of Solution A (2% (v/v) ACN in 0.1% (v/v) formic acid) and Solution B (80% (v/v) ACN in 0.1% (v/v) formic acid). The peptides were separated using a linear gradient of 4% B up to 40% B in 340 min with a flow rate of 300 nL/min. The column was placed in an oven at 35 °C.

LC-MS/MS

Eluted peptides were ionized by a nanospray source and detected by an LTQ Orbitrap XL mass spectrometer (Thermo Fisher Scientific, Waltham, MA, USA) operating in a data dependent mode (DDA). Full scan MS spectra were acquired in the orbitrap (m/z 300–1600) in profile mode with resolution set to 60,000 at m/z 400 and automatic gain control target at 106 ions. The six most intense ions were sequentially isolated for collision-induced (CID) MS/MS fragmentation and detection in the linear ion trap. Dynamic exclusion was set to 1 min and activated for 90 sec. Ions with single charge states were excluded. Lockmass of m/z 445,120025 was used for continuous internal calibration. XCalibur (Thermo Scientific) was used to control the system and acquire the raw files.

Protein identification and quantification

The raw mass spectral files were processed using MaxQuant software (version 1.6.9.0) with default parameters for protein identification and quantification. Trypsin specificity was set to allow two missed cleavages and minimum peptide length was set to 7 amino acids. Cysteine carbamidomethylation was set as fixed, and methionine oxidation, deamidation of asparagine and glutamine and N-terminal acetylation were set as variable modifications. A maximum of 5 modifications per peptide was set. The false discovery rate both for peptide and protein was set to 1%. For calculation of protein abundances, label-free quantification (LFQ) was performed with both "second peptides" and "match between run" options enabled. The human FASTA files were from UniProt downloaded on 15 October 2019.

Proteomic data analysis

Statistical analysis was performed using Perseus (1.6.6.0). Proteins identified as contaminants, "reverse" and "only identified by site" were filtered out. The LFQ intensities were transformed to logarithmic values [log2(x)]. The protein groups were filtered to obtain at least 2 valid values in at least one group. The label-free quantified proteins were subjected to statistical analysis with ANOVA test (permutation-based p-value with 0.05 cutoff). LC-MS/MS data after statistical analysis were plotted in a volcano graph based on the

difference between the two samples expressed as log2(x) versus their statistical significance expressed as −Log10(p-value). Hierarchical clustering was carried out on Z-score transformed LFQ values using average linkage of Euclidian distance. For statistical and bioinformatics analysis, as well as for visualization, Perseus, which is part of Maxquant, was used[80]. GO Enrichment analysis for biological processes, molecular function and cellular compartment was performed using DAVID functional annotation tools with official gene symbol as identifiers, the Homo sapiens background and the GOTERM_DIRECT annotation categories. A P value of 0.05 was selected as the cutoff criterion. The enrichment of proteins involved in signaling pathways was performed using the Reactome pathway database. A P value of 0.01 was selected as the cutoff criterion.

Western blot

Cells were lysed at 4 °C for 15 min in ice cold lysis buffer [150mMNaCl, 50 mM Tris pH 7.5, 1% Triton X-100, 1 mM EDTA, 1 mM EGTA, 0.1% SDS, 0.5% sodium deoxycholate containing PhosSTOP phosphatase inhibitors and a complete protease inhibitor mixture (Roche Life Science)], and centrifuged at 20,000 g. Protein concentration was estimated in the supernatant by Bradford assay (Applichem). Proteins were separated by SDS-polyacrylamide gel electrophoresis and transferred onto nitrocellulose membranes (Maine Manufacturing). For phospho-(Ser129)-αSyn detection, the membrane was heated at 65 °C overnight in PBS. Nonspecific binding sites were blocked in TBS/ 0.1% Tween 20/ 5% skimmed milk for 1 hour at 20 °C followed by overnight incubation with primary antibodies diluted in the same buffer. Incubation with appropriate HRP-conjugated secondary antibodies (Thermo) was for 2 hours at room temperature and protein bands were visualized using the Clarity Western ECL Substrate (BIO-RAD). Densitometric analysis was performed using ImageJ software (NIH). All blots were derived from the same experiment and were processed in parallel. Original unprocessed blots are shown in Supplementary Fig. 7.

Production of CMV.DsRed and CMV.DsRed.A53T lentiviral vectors

Four plasmids were used for lentivirus generation: the lentiviral transfer vector and three lentiviral packaging vectors (pMDL, pRev and pVSVG; provided by Dr. Fred Gage, the Salk Institute for Biological Studies). The lentiviral transfer vectors for expression of either the red fluorescent protein DsRed under the control of CMV promoter (LV.CMV.DsRed) or for co-expression of the red fluorescent protein DsRed, a T2A bicistronic configuration and human p.A53T-αSyn under the control of CMV promoter (LV.CMV.DsRed.T2A.A53T) were constructed by VectorBuilder. The preparation and purification of the lentiviral vectors were performed as previously described[81].

Generation of stably transduced SH-SY5Y cells

SH-SY5Y cells were transduced with the control vector LV.CMV.DsRed or LV.CMV.DsRed.T2A.A53T for expression of DsRed or co- expression of DsRed and human p.A53T-αSyn. Transduced cells were maintained in regular RPMI 1640 medium/ 10% FBS (Gibco)/ 1% penicillin/streptomycin (Life Technologies) for 48 h with one change of medium, and were then transferred in selection medium containing 300 µg/ml gentamycin-disulfate G418. After 3 weeks of selection, when 100% of cells expressed the DsRED protein, they were frozen as a polyclonal pool.

Differentiation of SH-SY5Y cells

Cells were plated on PLL/Laminin coated plates (2×10^4 cells/cm^2) in regular RPMI 1640 medium/ 5% FBS/ 1% penicillin/streptomycin (DIV 0). The following day, 10 µM Retinoic Acid (RA) was added (DIV1). On DIV3, the medium was changed to Neurobasal supplemented with B27, N2, Glutamax and BDNF (50 ng/ml) with fresh medium added every 2-3 days until DIV9.

Cell culture and transfection of an inducible SH-SY5Y line expressing human p.A53T-αSyn

The inducible SH-SY5Y cell line, in which expression of p.A53T-αSyn was switched off in the presence of doxycycline (Dox, 2 µg/mL), was previously reported[59]. Transfection with GFP-LC3 or mCherry-GFP-p62 plasmids (provided by Dr Tamotsu Yoshimori, Osaka University, Japan and Dr Terje Johansen, University of Tromso, Norway, respectively) was performed in the absence of Dox using Lipofectamine 2000, according to the manufacturer's protocol (Invitrogen; Thermo Fisher Scientific, Inc.).

Protein synthesis assay

For detection of total protein synthesis, an assay Kit (ab239725; Abcam) was used that utilizes a cell permeable analog of puromycin, which once inside the cell, stops translation by forming covalent conjugates with nascent polypeptide chains. Truncated polypeptides can be detected based on a click reaction with fluorescent azide. Cells were pre-treated with DMSO vehicle or BX795 for different time points and were incubated for 2 h with fresh aliquots of media containing either Protein Label or Protein Label and BX795. Cyclohexamide that blocks protein synthesis was used as a negative control. Fluorescence images were acquired using a Leica TCS SP8 confocal microscope (LEICA Microsystems) and analyzed using ImageJ software (NIH).

Autophagy detection assay

For detection of autophagosomes and monitoring autophagic flux, cells were seeded in 48-well plates on coverslips. After 7d incubation, the cells were treated with BX795 (1uM). The Cyto-ID® autophagy detection kit (Enzo Life Sciences, Plymouth Meeting, PA) was used according to the manufacturer's instructions in live cells. Samples were briefly exposed to Cyto-ID Green Dye and Hoechst 33342 at 37 °C for 30 min. The cells were then washed with 1× assay buffer and fixed with 4% parafolmadehyde. Coverslips were mounted with ProLong Gold antifade reagent with DAPI (Cell Signaling) and images were acquired using a Leica TCS SP8 confocal microscope (LEICA Microsystems) and analyzed using ImageJ software (NIH).

P70 S6K kinase activity

A p70 S6K activity assay kit (ADI-EKS-470 Enzo Life Sciences) was used based on a solid phase enzyme-linked immunoabsorbent assay (ELISA) that utilizes a specific synthetic peptide as substrate for p70 S6K and a polyclonal antibody that recognizes the phosphorylated form of the substrate. The assay was developed according to the manufacturer's instructions. Briefly, purified recombinant kinase provided by the manufacturer was incubated in the absence or presence of the BX795 inhibitor for 30 min prior to initiating the kinase reaction. Rapamycin was used as a positive control. Samples were then transfered in a 96−well plate coated with the p70 S6K substrate, a synthesized peptide containing the S6 consensus sequence (KRRRLASLR) and the reaction was initiated with the addition of ATP. After removal of the reaction mixture and three washes, the plate was incubated with a phosphospecific substrate antibody (1:1000) for 1 h, followed by a secondary antibody conjugated to horseradish peroxidase (HRP) for 20 min. Color was developed using tetramethylbenzidine as substrate (TMB) and the absorbance was measured at 450 nm in a Bio-Rad 680 microplate reader.

Electron microscopy

For conventional electron microscopy, p.A53T patient-derived and control neurons were seeded on aclar film placed in glass petri dishes. The medium was replaced with pre-warmed fixative (2.5% glutaraldehyde in 0.1 M phosphate buffer) for 1 h. Cells were rinsed in buffer and post-fixed with 1% osmium tetroxide at 4 °C for 1 hour. The samples were dehydrated in a graded series of ethanol, followed by propylene oxide (PO). Cells were further processed for infiltration in a mixture of Epon/Araldite resins diluted in PO and were flat-embedded in fresh epoxy resin mixture. Finally, the specimens were allowed to polymerize at 60 °C for 24 h. Small epoxy pieces were peeled away from the petri dishes, glued on epoxy blocks for sectioning and were allowed to polymerize for additional 24 h. Ultrathin sections were cut with a Diatome diamond knife at a thickness of 65 nm on a Leica EM UC7 ultramicrotome and stained with uranyl acetate and lead citrate. Sections were examined with a Philips 420 transmission electron microscope and photographed with a Megaview G2 CCD camera.

Statistics

All experiments were replicated at least three times and data from parallel cultures were acquired. Statistical analysis was performed using GraphPad Prism 6 software. Before performing parametric tests, data were assessed for normality with a D'Agostino–Pearson omnibus. Statistical significance was calculated for two groups using Student's *t* tests or the Mann–Whitney test for non-parametric distribution. Group comparisons of data were performed by one-way ANOVA test followed by Tukey post hoc test using PRISM (Graph Pad). *P* values < 0.05 were considered significant; $*p < 0.05$, $**p < 0.01$, $***p < 0.001$, $****p < 0.0001$.

Reporting summary

Further information on research design is available in the Nature Research Reporting Summary linked to this article.

DATA AVAILABILITY

The mass spectrometry proteomics data have been deposited to the ProteomeXchange Consortium via the PRIDE partner repository with the dataset identifier PXD019574. All data needed to evaluate the conclusions in the paper are present in the paper and/or the Supplementary Materials. The raw and analyzed datasets generated during the study are available for research purposes from the corresponding author on reasonable request. Additional data related to this paper may be requested from the authors.

Received: 8 April 2021; Accepted: 12 January 2022;
Published online: 11 February 2022

REFERENCES

1. Baker, M. G. & Graham, L. The journey: Parkinson's disease. *BMJ* **329**, 611–614 (2004).
2. Olanow, C. W. & Tatton, W. G. Etiology and pathogenesis of Parkinson's disease. *Annu. Rev. Neurosci.* **22**, 123–144 (1999).
3. Pfeiffer, R. F. Non-motor symptoms in Parkinson's disease. *Parkinsonism Relat. Disord.* **22**, S119–S122 (2016).
4. Gibb, W. Idiopathic Parkinson's disease and the Lewy body disorders. *Neuropathol. Appl. Neurobiol.* **12**, 223–234 (1986).
5. Lewandowsky, M. H. *Handbuch* der neurologie: bd. Spezielle Neurologie IV, (J. Spring, 1914).
6. Baba, M. et al. Aggregation of alpha-synuclein in Lewy bodies of sporadic Parkinson's disease and dementia with Lewy bodies. *Am. J. Pathol.* **152**, 879–884 (1998).
7. Breydo, L., Wu, J. W. & Uversky, V. N. Alpha-synuclein misfolding and Parkinson's disease. *Biochimica et. biophysica acta* **1822**, 261–285 (2012).
8. Chartier-Harlin, M. C. et al. Alpha-synuclein locus duplication as a cause of familial Parkinson's disease. *Lancet* **364**, 1167–1169 (2004).
9. Petrucci, S., Ginevrino, M. & Valente, E. M. Phenotypic spectrum of alpha-synuclein mutations: New insights from patients and cellular models. *Parkinsonism Relat. Disord.* **22**, S16–S20 (2016).
10. Simon-Sanchez, J. et al. Genome-wide association study reveals genetic risk underlying Parkinson's disease. *Nat. Genet*. **41**, 1308–1312 (2009).
11. Conway, K. A. et al. Acceleration of oligomerization, not fibrillization, is a shared property of both alpha-synuclein mutations linked to early-onset Parkinson's disease: implications for pathogenesis and therapy. *Proc. Natl. Acad. Sci. USA* **97**, 571–576 (2000).
12. Duda, J. E. et al. Concurrence of alpha-synuclein and tau brain pathology in the Contursi kindred. *Acta neuropathologica* **104**, 7–11 (2002).
13. Kotzbauer, P. T. et al. Fibrillization of alpha-synuclein and tau in familial Parkinson's disease caused by the A53T alpha-synuclein mutation. *Exp. Neurol.* **187**, 279–288 (2004).
14. Cotzias, G. C., Van Woert, M. H. & Schiffer, L. M. Aromatic amino acids and modification of parkinsonism. *N. Engl. J. Med* **276**, 374–379 (1967).
15. Ghosh, D., Mehra, S., Sahay, S., Singh, P. K. & Maji, S. K. Alpha-synuclein aggregation and its modulation. *Int. J. Biol. Macromol.* **100**, 37–54 (2017).
16. Ghosh, D. et al. The Parkinson's disease-associated H50Q mutation accelerates alpha-Synuclein aggregation in vitro. *Biochemistry* **52**, 6925–6927 (2013).
17. Schulz-Schaeffer, W. J. The synaptic pathology of alpha-synuclein aggregation in dementia with Lewy bodies, Parkinson's disease and Parkinson's disease dementia. *Acta Neuropathologica* **120**, 131–143 (2010).
18. Chen, M. et al. Common proteomic profiles of induced pluripotent stem cell-derived three-dimensional neurons and brain tissue from Alzheimer patients. *J. Proteom.* **182**, 21–33 (2018).
19. Cooper, O. et al. Pharmacological rescue of mitochondrial deficits in iPSC-derived neural cells from patients with familial Parkinson's disease. *Sci. Transl. Med.* **4**, 141ra190 (2012).
20. Ryan, S. D. et al. Isogenic human iPSC Parkinson's model shows nitrosative stress-induced dysfunction in MEF2-PGC1alpha transcription. *Cell* **155**, 1351–1364 (2013).
21. Yang, Y. M. et al. A small molecule screen in stem-cell-derived motor neurons identifies a kinase inhibitor as a candidate therapeutic for ALS. *Cell Stem Cell* **12**, 713–726 (2013).
22. Kouroupi, G. et al. Defective synaptic connectivity and axonal neuropathology in a human iPSC-based model of familial Parkinson's disease. *Proc. Natl. Acad. Sci. USA* **114**, E3679–E3688 (2017).
23. Chambers, S. M. et al. Highly efficient neural conversion of human ES and iPS cells by dual inhibition of SMAD signaling. *Nat. Biotechnol.* **27**, 275–280 (2009).
24. Soldner, F. et al. Parkinson's disease patient-derived induced pluripotent stem cells free of viral reprogramming factors. *Cell* **136**, 964–977 (2009).
25. Lovestone, S. et al. A phase II trial of tideglusib in Alzheimer's disease. *J. Alzheimers Dis.* **45**, 75–88 (2015).
26. Pagan, F. L. et al. Pharmacokinetics and pharmacodynamics of a single dose Nilotinib in individuals with Parkinson's disease. *Pharm. Res. Perspect.* **7**, e00470 (2019).
27. Cuny, G. D. Kinase inhibitors as potential therapeutics for acute and chronic neurodegenerative conditions. *Curr. Pharm. Des.* **15**, 3919–3939 (2009).
28. Yu, T. et al. The kinase inhibitor BX795 suppresses the inflammatory response via multiple kinases. *Biochemical Pharmacol.* **174**, 113797 (2020).
29. Clark, K., Plater, L., Peggie, M. & Cohen, P. Use of the pharmacological inhibitor BX795 to study the regulation and physiological roles of TBK1 and IkappaB kinase epsilon: a distinct upstream kinase mediates Ser-172 phosphorylation and activation. *J. Biol. Chem.* **284**, 14136–14146 (2009).
30. Jaishankar, D. et al. An off-target effect of BX795 blocks herpes simplex virus type 1 infection of the eye. *Sci. Transl. Med.* **10**, eaan5861 (2018).
31. Su, A. R. et al. BX-795 inhibits HSV-1 and HSV-2 replication by blocking the JNK/p38 pathways without interfering with PDK1 activity in host cells. *Acta Pharm. Sin.* **38**, 402–414 (2017).
32. Zygogianni, O. et al. In vivo phenotyping of familial Parkinson's disease with human induced pluripotent stem cells: a proof-of-concept study. *Neurochem. Res.* **44**, 1475–1493 (2019).
33. Ryan, T. et al. Cardiolipin exposure on the outer mitochondrial membrane modulates alpha-synuclein. *Nat. Commun.* **9**, 817 (2018).
34. Walker, D. G. et al. Changes in properties of serine 129 phosphorylated alpha-synuclein with progression of Lewy-type histopathology in human brains. *Exp. Neurol.* **240**, 190–204 (2013).
35. Bai, L. Y. et al. BX795, a TBK1 inhibitor, exhibits antitumor activity in human oral squamous cell carcinoma through apoptosis induction and mitotic phase arrest. *Eur. J. Pharm.* **769**, 287–296 (2015).
36. Cox, J. et al. Accurate proteome-wide label-free quantification by delayed normalization and maximal peptide ratio extraction, termed MaxLFQ. *Mol. Cell Proteom.* **13**, 2513–2526 (2014).
37. Cox, J. & Mann, M. MaxQuant enables high peptide identification rates, individualized p.p.b.-range mass accuracies and proteome-wide protein quantification. *Nat. Biotechnol.* **26**, 1367–1372 (2008).
38. Chung, C. Y. et al. In situ peroxidase labeling and mass-spectrometry connects alpha-synuclein directly to endocytic trafficking and mRNA metabolism in neurons. *Cell Syst.* **4**, 242–250 (2017). e244.
39. Bowden, H. A. & Dormann, D. Altered mRNP granule dynamics in FTLD pathogenesis. *J. neurochemistry* **138**, 112–133 (2016).
40. Kapur, M., Monaghan, C. E. & Ackerman, S. L. Regulation of mRNA translation in. *Neurons-A Matter Life Death. Neuron* **96**, 616–637 (2017).
41. Chung, C. Y. et al. Identification and rescue of alpha-synuclein toxicity in Parkinson patient-derived neurons. *Science* **342**, 983–987 (2013).
42. Khurana, V. et al. Genome-scale networks link neurodegenerative disease genes to alpha-synuclein through specific molecular pathways. *Cell Syst.* **4**, 157–170 (2017). e114.
43. Carpanini, S. M. et al. A novel mouse model of Warburg Micro syndrome reveals roles for RAB18 in eye development and organisation of the neuronal cytoskeleton. *Dis. Model Mech.* **7**, 711–722 (2014).
44. Feldmann, A. et al. The RAB GTPase RAB18 modulates macroautophagy and proteostasis. *Biochem Biophys. Res. Commun.* **486**, 738–743 (2017).
45. Rocca, D. L. et al. The small GTPase Arf1 modulates Arp2/3-mediated actin polymerization via PICK1 to regulate synaptic plasticity. *Neuron* **79**, 293–307 (2013).
46. Jean, S., Cox, S., Nassari, S. & Kiger, A. A. Starvation-induced MTMR13 and RAB21 activity regulates VAMP8 to promote autophagosome-lysosome fusion. *EMBO Rep.* **16**, 297–311 (2015).
47. Farley, M. M. & Watkins, T. A. Intrinsic neuronal stress response pathways in injury and disease. *Annu Rev. Pathol.* **13**, 93–116 (2018).
48. Maraganore, D. M. et al. UCHL1 is a Parkinson's disease susceptibility gene. *Ann. Neurol.* **55**, 512–521 (2004).
49. Williams, E. T., Chen, X. & Moore, D. J. VPS35, the retromer complex and Parkinson's disease. *J. Parkinsons Dis.* **7**, 219–233 (2017).
50. Chi, B. et al. The neurodegenerative diseases ALS and SMA are linked at the molecular level via the ASC-1 complex. *Nucleic Acids Res.* **46**, 11939–11951 (2018).
51. Abramzon, Y. A., Fratta, P., Traynor, B. J. & Chia, R. The overlapping genetics of amyotrophic lateral sclerosis and frontotemporal dementia. *Front Neurosci.* **14**, 42 (2020).
52. Gonzalez, M. A. et al. A novel mutation in VCP causes Charcot-Marie-Tooth Type 2 disease. *Brain* **137**, 2897–2902 (2014).
53. Aminkeng, F. HINT1 mutations define a novel disease entity - autosomal recessive axonal neuropathy with neuromyotonia. *Clin. Genet* **83**, 31–32 (2013).
54. Haverfield, E. V., Whited, A. J., Petras, K. S., Dobyns, W. B. & Das, S. Intragenic deletions and duplications of the LIS1 and DCX genes: a major disease-causing

mechanism in lissencephaly and subcortical band heterotopia. *Eur. J. Hum. Genet* **17**, 911–918 (2009).
55. Bernert, G., Fountoulakis, M. & Lubec, G. Manifold decreased protein levels of matrin 3, reduced motor protein HMP and hlark in fetal Down's syndrome brain. *Proteomics* **2**, 1752–1757 (2002).
56. Shima, H. et al. Disruption of the p70(s6k)/p85(s6k) gene reveals a small mouse phenotype and a new functional S6 kinase. *EMBO J.* **17**, 6649–6659 (1998).
57. Parekh, P. et al. A cleaning crew: the pursuit of autophagy in Parkinson's disease. *ACS Chem. Neurosci.* **10**, 3914–3926 (2019).
58. Rabanal-Ruiz, Y., Otten, E. G. & Korolchuk, V. I. mTORC1 as the main gateway to autophagy. *Essays Biochem* **61**, 565–584 (2017).
59. Xilouri, M., Vogiatzi, T., Vekrellis, K., Park, D. & Stefanis, L. Abberant alpha-synuclein confers toxicity to neurons in part through inhibition of chaperone-mediated autophagy. *PLoS One* **4**, e5515 (2009).
60. Kabeya, Y. et al. LC3, a mammalian homologue of yeast Apg8p, is localized in autophagosome membranes after processing. *EMBO J.* **19**, 5720–5728 (2000).
61. Jiang, P. & Mizushima, N. LC3- and p62-based biochemical methods for the analysis of autophagy progression in mammalian cells. *Methods* **75**, 13–18 (2015).
62. Lopez, A., Fleming, A. & Rubinsztein, D. C. Seeing is believing: methods to monitor vertebrate autophagy in vivo. *Open Biology* **8**, 180106 (2018).
63. Pankiv, S. et al. p62/SQSTM1 binds directly to Atg8/LC3 to facilitate degradation of ubiquitinated protein aggregates by autophagy. *J. Biol. Chem.* **282**, 24131–24145 (2007).
64. Spira, P. J., Sharpe, D. M., Halliday, G., Cavanagh, J. & Nicholson, G. A. Clinical and pathological features of a Parkinsonian syndrome in a family with an Ala53Thr alpha-synuclein mutation. *Ann. Neurol.* **49**, 313–319 (2001).
65. Yamaguchi, K. et al. Abundant neuritic inclusions and microvacuolar changes in a case of diffuse Lewy body disease with the A53T mutation in the alpha-synuclein gene. *Acta Neuropathologica* **110**, 298–305 (2005).
66. Yeo, G., Holste, D., Kreiman, G. & Burge, C. B. Variation in alternative splicing across human tissues. *Genome Biol.* **5**, R74 (2004).
67. Apicco, D. J. et al. Dysregulation of RNA splicing in tauopathies. *Cell Rep.* **29**, 4377–4388 (2019). e4374.
68. Garcia-Esparcia, P. et al. Altered machinery of protein synthesis is region- and stage-dependent and is associated with alpha-synuclein oligomers in Parkinson's disease. *Acta Neuropathologica Commun.* **3**, 76 (2015).
69. Johnson, S. C., Rabinovitch, P. S. & Kaeberlein, M. mTOR is a key modulator of ageing and age-related disease. *Nature* **493**, 338–345 (2013).
70. Kim, J. & Guan, K. L. mTOR as a central hub of nutrient signalling and cell growth. *Nat. Cell Biol.* **21**, 63–71 (2019).
71. Papadopoli, D. et al. mTOR as a central regulator of lifespan and aging. *F1000Res* **8**, 998 (2019).
72. Xun, Z., Sowell, R. A., Kaufman, T. C. & Clemmer, D. E. Quantitative proteomics of a presymptomatic A53T alpha-synuclein Drosophila model of Parkinson disease. *Mol. Cell Proteom.* **7**, 1191–1203 (2008).
73. Fernandez-Santiago, R. et al. SNCA and mTOR pathway single nucleotide polymorphisms interact to modulate the age at onset of Parkinson's Disease. *Mov. Disord.* **34**, 1333–1344 (2019).
74. Arotcarena, M. L., Teil, M. & Dehay, B. Autophagy in synucleinopathy: the overwhelmed and defective machinery. *Cells* **8**, 565 (2019).
75. Menzies, F. M. et al. Autophagy and neurodegeneration: pathogenic mechanisms and therapeutic opportunities. *Neuron* **93**, 1015–1034 (2017).
76. Oakes, J. A., Davies, M. C. & Collins, M. O. TBK1: a new player in ALS linking autophagy and neuroinflammation. *Mol. Brain* **10**, 5 (2017).
77. Pietri, M. et al. PDK1 decreases TACE-mediated alpha-secretase activity and promotes disease progression in prion and Alzheimer's diseases. *Nat. Med.* **19**, 1124–1131 (2013).
78. Dorval, T. et al. Contextual automated 3D analysis of subcellular organelles adapted to high-content screening. *J. Biomol. Screen.* **15**, 847–857 (2010).
79. Hughes, C. S. et al. Single-pot, solid-phase-enhanced sample preparation for proteomics experiments. *Nat. Protoc.* **14**, 68–85 (2019).
80. Tyanova, S. et al. The perseus computational platform for comprehensive analysis of (prote)omics data. *Nat. Methods* **13**, 731–740 (2016).
81. Tiscornia, G., Singer, O. & Verma, I. M. Production and purification of lentiviral vectors. *Nat. Protoc.* **1**, 241–245 (2006).

ACKNOWLEDGEMENTS

We thank Drs. Tamotsu Yoshimori and Terje Johansen for providing GFP-LC3 and mCherry-GFP-p62 plasmids, respectively. This work was supported by: a Stavros Niarchos Foundation grant to the Hellenic Pasteur Institute as part of the Foundation's initiative to support the Greek Research Center ecosystem; the Greek General Secretariat for Research and Technology (GSRT) grant BIOIMAGING-GR MIS 5002755 implemented under the Action "Reinforcement of Research and Innovation Infrastructure", and EATRIS-GR OPS5028091, both funded by the Operational Programme "Competitiveness, Entrepreneurship and Innovation" (NSRF 2014-2020) and co-financed by Greece and the European Union (European Regional Development Fund); the GSRT Flagship Action for Neurodegenerative Diseases on the basis of Personalized Medicine; the Hellenic Foundation for Research and Innovation (HFRI) 899-PARKINSynapse grant to G.K and HFRI 1019-DiseasePhenoTarget grant to R.M.; the South Korea Ministry of Science and ICT (MSIT) grant (NRF-2017M3A9G6068257) to RG. N.A. was recipient of a Calmette & Yersin Fellowship for a technology exchange visit to the Institut Pasteur Korea.

AUTHOR CONTRIBUTIONS

N.A. carried out the experiments analyzed and interpreted the data, generated the figures, participated in the study design and in writing the manuscript. K.P. and E.T. analyzed proteomics data. G.K. generated the patient-derived p.A53T and control iPSCs used in this study and provided training on iPSC culture and differentiation. I.B. participated in some experiments involving cell culture and confocal microscopy, phenotype analysis and quantification. M.S. and G.P. performed the proteomic analysis. M.X. and L.S. provided reagents, analytic tools and guidance for autophagy experiments. I.K. performed electron microscopy and interpretation. N.A. and R.G. performed high-content imaging and drug screening on p.A53T neurons. E.T. and R.M. conceived, designed and supervised the study, analyzed the data and wrote the paper with contribution from all authors.

COMPETING INTERESTS

The authors declare no competing interests.

ADDITIONAL INFORMATION

Supplementary information The online version contains supplementary material available at https://doi.org/10.1038/s41531-022-00278-y.

Correspondence and requests for materials should be addressed to Rebecca Matsas.

Reprints and permission information is available at http://www.nature.com/reprints

Publisher's note Springer Nature remains neutral with regard to jurisdictional claims in published maps and institutional affiliations.